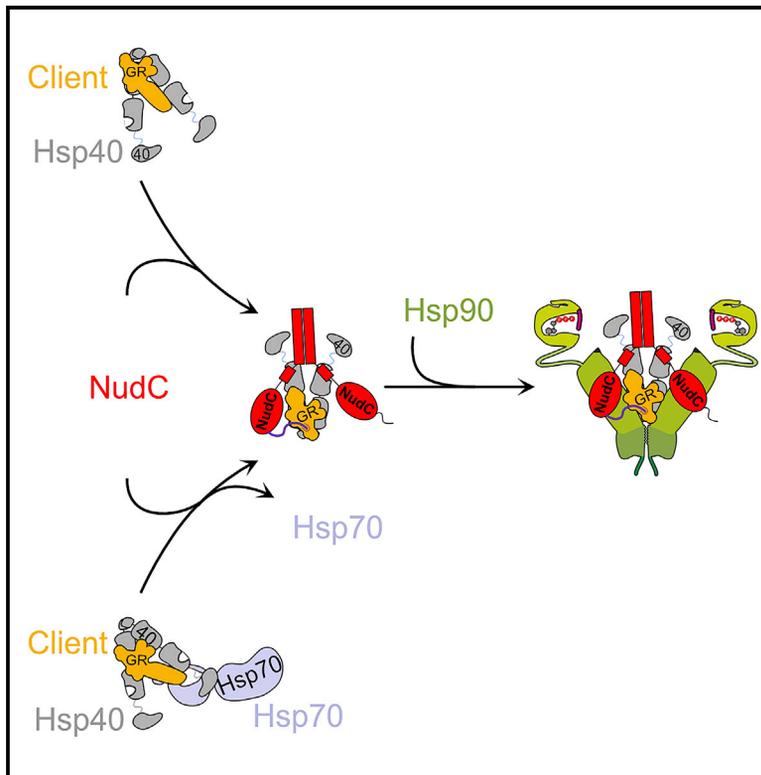# NudC guides client transfer between the Hsp40/70 and Hsp90 chaperone systems

Graphical abstract

Authors

Maximilian M. Biebl,
Florent Delhommel, Ofrah Faust, ...,
Rina Rosenzweig, Michael Sattler,
Johannes Buchner

Correspondence

sattler@helmholtz-muenchen.de (M.S.),
johannes.buchner@tum.de (J.B.)

In brief

Structural and biochemical analyses revealed that the protein NudC supports the transfer of substrate proteins from the Hsp70/Hsp40 chaperone machinery to Hsp90 with a unique mechanism. NudC binds to Hsp40, the substrate protein, and excludes Hsp70 from the complex. The interaction of NudC with Hsp90 results in substrate handover and activation.

Highlights

- NudC is required for viability and substrate protein activation in mammalian cells

- NudC recruits Hsp40-bound protein substrates to Hsp90 and promotes their activation

- NudC excludes Hsp70 from substrate complexes

- NudC transfer recruits Hsp40-complexes, while the Hop pathway focuses on Hsp70

CelPress

Article

NudC guides client transfer between the Hsp40/70 and Hsp90 chaperone systems

Maximilian M. Biebl,[1,7] Florent Delhommel,[1,2,7] Ofrah Faust,[3] Krzysztof M. Zak,[2] Ganesh Agam,[4] Xiaoyan Guo,[5,6] Moritz Mühlhofer,[1] Vinay Dahiya,[1] Daniela Hillebrand,[1] Grzegorz M. Popowicz,[2] Martin Kampmann,[5,6] Don C. Lamb,[4] Rina Rosenzweig,[3] Michael Sattler,[1,2,*] and Johannes Buchner[1,8,*]

[1]Department of Chemistry, Technische Universität München, Lichtenbergstrasse 4, 85747 Garching, Germany
[2]Institute of Structural Biology, Helmholtz Zentrum München, Neuherberg, Germany
[3]Department of Structural Biology, Weizmann Institute of Science, Rehovot, Israel
[4]Department of Chemistry, Ludwig-Maximilians-Universität München, München, Germany
[5]Institute for Neurodegenerative Diseases University of California, San Francisco, CA, USA
[6]Department for Biochemistry and Biophysics, University of California, San Francisco, CA, USA
[7]These authors contributed equally
[8]Lead contact
*Correspondence: sattler@helmholtz-muenchen.de (M.S.), johannes.buchner@tum.de (J.B.)
https://doi.org/10.1016/j.molcel.2021.12.031

SUMMARY

In the eukaryotic cytosol, the Hsp70 and the Hsp90 chaperone machines work in tandem with the maturation of a diverse array of client proteins. The transfer of nonnative clients between these systems is essential to the chaperoning process, but how it is regulated is still not clear. We discovered that NudC is an essential transfer factor with an unprecedented mode of action: NudC interacts with Hsp40 in Hsp40-Hsp70-client complexes and displaces Hsp70. Then, the interaction of NudC with Hsp90 allows the direct transfer of Hsp40-bound clients to Hsp90 for further processing. Consistent with this mechanism, NudC increases client activation *in vitro* as well as in cells and is essential for cellular viability. Together, our results show the complexity of the cooperation between the major chaperone machineries in the eukaryotic cytosol.

INTRODUCTION

Molecular chaperones have evolved not only to support the correct folding and maturation of proteins, called clients, into their native, active conformation, but also to prevent deleterious misfolding and aggregation (Balchin et al., 2016). Among molecular chaperones, heat shock protein 70 (Hsp70) and heat shock protein 90 (Hsp90) closely collaborate in the processing of a diverse spectrum of clients involved in many aspects of cellular function (Echeverría et al., 2011). Hsp70 and the associated Hsp40/J-domain protein (JDP) co-chaperones (hereafter referred to as Hsp40) unfold proteins in an ATP-dependent manner. Together, they play a pivotal role in facilitating the *de novo* folding of proteins, preventing protein aggregation and re-solubilizing aggregated proteins (Faust et al., 2020; Mayer and Bukau, 2005; Rosenzweig et al., 2019; Wentink et al., 2020). For many clients, the coordinated transfer to Hsp90 is required to reach their native, fully folded state (Boysen et al., 2019; Dahiya et al., 2019; Morán Luengo et al., 2018). Notably, Hsp70 binds to clients more promiscuously than Hsp90, which is predominantly involved in the late stages of maturation.

Hsp70 comprises an N-terminal nucleotide-binding domain (NBD) and a C-terminal substrate-binding domain (SBD). The client binding site of Hsp70 cycles between high- and low-affinity states, which is controlled in an ATP-dependent manner by the conformational changes of a lid subdomain. The ATPase activity

is slow and, thus, provides considerable scope for regulation by co-chaperones, such as Hsp40 proteins and nucleotide exchange factors (NEFs). Hsp40s bind to clients and target them to Hsp70. All Hsp40s comprise an eponymous J-domain, and most class A and class B Hsp40s additionally contain a G/F-rich linker, CTD-I and CTD-II regions involved in substrate binding, and a C-terminal dimerization domain (Rosenzweig et al., 2019). All Hsp40s interact with Hsp70 through their J-domain, causing a dramatic increase in the Hsp70 ATPase activity. In addition, some Hsp40s also bind the C-terminal EEVD motif of Hsp70 with their C-terminal domains (CTDs), which is important for the activation of these Hsp40 proteins (Aron et al., 2005; Faust et al., 2020; Jiang et al., 2019).

Hsp90 consists of an NTD, which is connected to the middle domain (MD) via a long, charged linker. The CTD mediates dimerization (Ali et al., 2006; Hainzl et al., 2009; Prodromou et al., 1997). Hsp90 undergoes an ATP-driven conformational cycle from open to closed states in which the NTDs transiently dimerize and associate with the MD to complete the ATPase site (Hessling et al., 2009; Prodromou et al., 2000). Importantly, a plethora of co-chaperones assist and regulate Hsp90 function (Biebl and Buchner, 2019). Hsp90's co-chaperones have significantly expanded throughout evolution with 12 known in yeast and more than 20 known in man (Johnson, 2012). Co-chaperones can associate with Hsp90 in a client-specific manner or at different stages of the Hsp90 conformational cycle. In

addition, many of them also have Hsp90-independent functions (Bose et al., 1996; Echtenkamp et al., 2016; Freeman and Morimoto, 1996; Grammatikakis et al., 1999; Li et al., 2011).

The Hsp70-Hsp90 organizing protein (Hop) associates via its TPR domains with the C-terminal EEVD motifs of both Hsp70 and Hsp90 (Chen and Smith, 1998; Johnson et al., 1998). Thus, Hop acts as a physical connector between these chaperones and facilitates client handover (Röhl et al., 2015; Wegele et al., 2006). Additionally, Hop is a noncompetitive Hsp90 ATPase inhibitor that keeps Hsp90 in a partially opened, client-accessible conformational state (Prodromou et al., 1999; Richter et al., 2003; Schmid et al., 2012). Notably, in yeast, it was found that Hop is only required for a subset of clients (Sahasrabudhe et al., 2017). Furthermore, a recent study suggests that most Hsp90 clients remain unaffected by the knockout of Hop in mammalian cells, raising the question whether other transfer mechanisms between Hsp70 and Hsp90 exist (Bhattacharya et al., 2020). Direct contacts between Hsp70 and Hsp90 occur in yeast as well as in bacteria that generally lack Hsp90 co-chaperones; but so far direct contacts for the mammalian system have only been shown under crosslinking conditions (Genest et al., 2015; Kravats et al., 2018; Wang et al., 2020).

The importance of an efficient substrate handover from Hsp70 to Hsp90 suggests that other factors could be involved in this process. We established a CRISPRi-based screening platform to search for the modulators of Hsp90 function and identified the nuclear migration protein NudC as a high-scoring hit. A previous large-scale study suggests that the nuclear migration protein NudC can interact with both Hsp70 and Hsp90 systems and could, thus, be of interest in the context of client recruitment to Hsp90 (Taipale et al., 2014). NudC is a 38-kDa protein composed of a unique NTD of unknown function, followed by a coiled-coil domain that is involved in dimerization, and a Cysteine- and histidine-rich domain (CHORD) and Sgt1 (CS) domain that is also found in the Hsp90 co-chaperones p23 and Sgt1 (Zheng et al., 2011). Accordingly, an interaction of NudC family proteins with Hsp90 has been shown (Fu et al., 2016; Yang et al., 2010; Zheng et al., 2011). However, to date, the co-chaperone functions of NudC have remained enigmatic. NudC potentially maintains the function of the dynein-motor-associated protein lissencephaly protein 1 (Lis1) together with Hsp90 (Ali et al., 1993; Yang et al., 2010; Zhu et al., 2010). NudC is ubiquitously expressed, and it is present in levels comparable with those of Hop in several cell lines (Finka and Goloubinoff, 2013). High concentrations of NudC are especially found in proliferating tissue and cancer cells, linking NudC to cancerogenesis (Gocke et al., 2000). Strongly increased NudC levels have been found in the bone marrow aspirates from patients with acute lymphoblastic leukemia and acute myelogenous leukemia compared with normal tissue (Fu et al., 2016; Gocke et al., 2000).

Here, we unravel that NudC is a functionally and structurally unique co-chaperone that directly interacts with Hsp40 and Hsp90 using independent binding sites. We show that it accelerates the client transfer from Hsp40/Hsp70 to Hsp90 by an unprecedented mechanism. The NudC activity is essential for the processing of clients such as the glucocorticoid receptor and p53, which are implicated in diseases such as mood disorders and cancer.

RESULTS

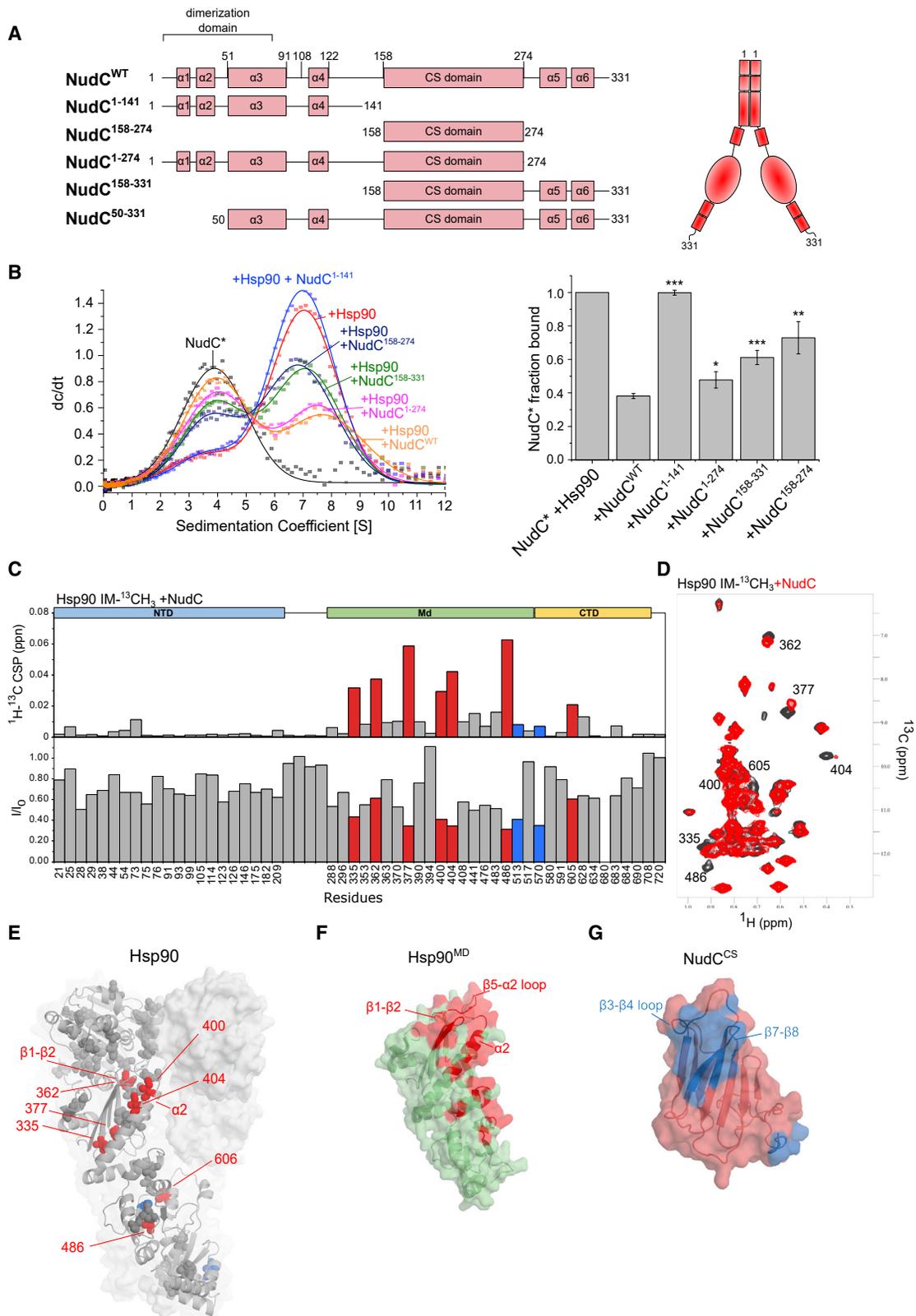### NudC modulates Hsp90 activity in cells

To identify Hsp90 modulators, we constructed a CRISPRi-based screening system (Gilbert et al., 2013; Qi et al., 2013) in which the GR is expressed constitutively and the functional GR drives the expression of the fluorescent reporter protein mCherry. Reporter activity was strongly activated by treatment with dexamethasone, which could be suppressed by the Hsp90 inhibitor geldanamycin (Figure S1A). We screened a library of single guide RNAs (sgRNAs) that target 357 genes involved in proteostasis for their effect on reporter levels (Figure 1A). We found p23 (*PTGES3*) as a potent activator of GR activity, matching its central role in steroid hormone receptor (SHR) maturation, which was observed in previous studies (Biebl et al., 2021; Dittmar et al., 1996; Freeman et al., 2000; Johnson and Toft, 1995; Sahasrabudhe et al., 2017). Hop (*STIP1*) was also identified as a positive regulator of GR but with a smaller effect. By contrast, FKBP51 (*FKBP5*) was found as a negative regulator of GR activity, in line with previous observations. Together, these findings confirm the validity of the screening approach to identify Hsp90-dependent SHR modulators. Notably, we identified the nuclear migration protein NudC as one of the highest-scoring hits leading to the loss of GR function when knocked down, suggesting that it plays a central role in GR maturation.

To validate the NudC as a modulator of GR activity, we transduced the screening cell line with individual sgRNA-expressing plasmids to knock down NudC. The knockdown of NudC strongly reduced the GR activation by dexamethasone compared with the control, confirming that NudC is important for the GR activation in cells (Figures 1B, S1B, and S1C). Importantly, we also found that the fraction of NudC-depleted cells decreased by approximately 80% within 11 days after virus infection, showing that the loss of NudC was toxic for K562 cells (Figure 1C). This suggests that NudC is involved in essential cellular processes. By contrast, although the knockdown efficiency for NudC and Hop was comparable, the knockdown of Hop only had a minor effect on GR activity in one of the tested sgRNAs and viability was only slightly affected in the other sgRNA, hinting at a weak off-target toxicity. Thus, Hop only weakly affected GR activity and viability, suggesting that Hop is not required for the maturation of many clients, matching previous findings (Bhattacharya et al., 2020; Biebl et al., 2020; Sahasrabudhe et al., 2017). In conclusion, these results suggest that NudC is essential to maintain GR activity and viability in the cellular context.

NudC interacts with Hsp90

Using NMR spectroscopy and analytical ultracentrifugation (aUC) experiments, we determined that the N-terminal helices α1-α3 mediate the NudC dimerization. The dimerization region is followed by the structurally independent helix α4, which is connected to the NudC-CS domain via a short linker. The C-terminal region harbors two long helices in line with previous predictions (Figures 2A and S2).

We next analyzed the interaction of NudC with Hsp90. Using SEC-MALS, we found that a NudC dimer binds one Hsp90 dimer with a 1:1 stoichiometry (Figure S3A). aUC revealed efficient

Figure 1. NudC affects GR activity *in vivo*

(A) CRISPR interference (CRISPRi) screen for SHR modulators. K562 cells that constitutively express GR and a GR-dependent mCherry reporter as well as the CRISPRi machinery (Gilbert et al., 2014) were transduced with an sgRNA library targeting 357 proteostasis genes. Cells were FACS-sorted based on reporter expression, and sgRNA frequencies in the populations with high and low reporter levels were compared by next-generation sequencing. Phenotypes based on $\log_2$-fold differences in sgRNA abundances between populations and p values were calculated for each gene as described in the STAR Methods and are shown as a volcano plot. Green data-points represent targeted genes, gray points indicate nontargeting controls. The 0.05 false-discovery rate threshold is indicated by a dashed line. Hsp90 co-chaperones producing significant hits are shown in blue, and NudC is highlighted in red.

(B) NudC maintains GR activity *in vivo*. CRISPRi was used to knock down NudC and Hop in the reporter cells. Median mCherry fluorescence was measured by flow cytometry as a readout for GR activity after the incubation with 10 nM dexamethasone for 24 h. The results represent means and SD of three biological replicates. Statistical significance was determined by student-t test (n.s. $p \geq 0.05$; * $p < 0.05$, ** $p < 0.01$, *** $p < 0.001$).

(C) NudC is important for cellular survival. NudC was depleted in K562 cells using CRISPRi. An sgRNA-encoding plasmid harboring a BFP marker was transduced by lentiviral infection on day 0, and the fraction of BFP^+ cells was determined by flow cytometry on the indicated days after infection. The results represent means and SD of three biological replicates.

binding of NudC Hsp90α and Hsp90β in various nucleotide states, suggesting a similar binding mode of NudC to both Hsp90 isoforms that is largely unaffected by the Hsp90 conformation (Figure S3A). The titration of Hsp90α to Atto488-labeled NudC (NudC*) in the absence of nucleotide revealed an apparent K_D of 650 nM (Figure S3C), a value comparable to other Hsp90 co-chaperones (Wandinger et al., 2006). To determine the effect of NudC on the Hsp90 ATPase, we used a regenerative ATPase assay (Ali et al., 1993). In line with the nucleotide-independent binding of NudC to Hsp90, NudC did not significantly affect the Hsp90 ATPase, thus opposing previous reports (Figures S3D and S3E) (Zhu et al., 2010). As a control, we confirmed the expected inhibitory effect of Hop and the simulating effect of Aha1 on the Hsp90 ATPase as previously published (Li et al., 2013; Schmid et al., 2012).

To map the region of NudC involved in Hsp90 binding, we used NudC fragments to test if they can displace the labeled full-length NudC (NudC*) from a preformed Hsp90:NudC* complex (Figures 2A and 2B). The addition of NudC^{WT} as a control reduced the fraction of bound NudC* by approximately 60%. The N-terminal NudC$^{1-141}$ construct did not bind to Hsp90. By contrast, the isolated CS domain NudC$^{158-274}$ was able to displace NudC*. Moreover, the NudC$^{158-331}$ fragment that harbors the two C-terminal

α-helices bound Hsp90 slightly better compared with the CS domain alone. Importantly, constructs encompassing the N-terminal dimerization domain resulted in significantly higher binding efficiencies. This indicates that the dimerization of NudC is not a prerequisite for the Hsp90 interaction but results in higher binding efficiency. Together, these results identify the NudC-CS domain as the main Hsp90-interacting domain with additional contributions from the C-terminal helices. The enhanced Hsp90 interaction in the presence of the N-terminal dimerization domain likely reflects avidity.

To determine which of the Hsp90 domains mediate the NudC interaction, we studied the interaction of full-length NudC with fragments of Hsp90 by aUC. We found that NudC binds both to Hsp90^{NTD-MD} and Hsp90^{MD-CTD}, suggesting that NudC interacts primarily with the MD of Hsp90 (Figure S4A). The NudC binding interfaces were mapped by NMR using Ile-Met $^{13}CH_3$-specific labeling of the full-length Hsp90 dimer (Figures 2C and 2D). Upon NudC binding, most of the perturbed residues are observed in the Hsp90 MD and are clustered in two regions (Figure 2E): Strongest chemical shift perturbations (CSPs) and line-broadening were observed for residues in close proximity to the interface of the β1-β2 hairpin with helix α2 in the Hsp90 MD. Additional, but smaller, spectral changes were found for residues in the MD/CTD interface

(legend on next page)

(Figure S4B). Experiments with truncations of NudC confirmed that the NudC-CS domain is the main Hsp90 interaction site, whereas the N-terminal dimerization region of NudC is not involved in the binding of Hps90 (Figures S4B–S4E). Mapping of the interaction with the individual ^{15}N-labeled Hsp90-MD, NudC$^{158-274}$, and NudC$^{158-331}$ confirmed these conclusions (Figures 2F and S4F–S4K).

Moreover, a reverse titration of Hsp90-MD to ^{15}N-labeled NudC$^{158-274}$ revealed a continuous binding surface on the NudC-CS domain, which comprises the β3-β4 loop (residues 189, 193–196, 197–198) and the β7-β8 strands (residues 232–239, 241–243) (Figures 2G and S4H–S4K).

Our NMR titration experiments indicate that the β1-β2 loop, the β5-α2 loop, and the N-terminal region of helix α2 in the Hsp90-MD interact with the β3-β4 loop and the β7-β8 strands of the NudC-CS domain. We generated a docking model of the Hsp90-MD/NudC-CS complex using HADDOCK (Dominguez et al., 2003). The structural model was experimentally validated with intermolecular paramagnetic relaxation enhancement (PRE) experiments using spin-labeled NudC-CS (Figure S5). Notably, the Hsp90-NudC^{CS} domain interface is distinct from the interaction of Hsp90 with CS domains of other co-chaperones (Ali et al., 2006; Zhang et al., 2008) and reflects differences in the primary sequence and surface properties of the NudC-CS domain. These unique features allow binding of NudC to both open and closed states of Hsp90, consistent with the fact that NudC can bind to different Hsp90 nucleotide states and does not affect the Hsp90 ATPase activity (Figures S3B and S3D).

NudC interacts with Hsp40 through an extended motif similar to the Hsp70 C terminus

Previous experiments (Taipale et al., 2014) suggests an interaction of NudC with the Hsp90 and Hsp70 systems in cells. Surprisingly, aUC analysis of the purified proteins did not show any interaction of NudC with Hsp70, neither in the presence nor in the absence of ATP (Figure S6A). By contrast, NudC interacted with yeast Hsp40 (Ydj1), showing a high binding affinity ($K_D \sim$ 800 nM) (Figures 3A and S6B). To show the conservation of the NudC-Hsp40 interaction, we also confirmed the binding of NudC to the human Hsp40 proteins DNAJA1 and DNAJB1 (Figure S6C). Although Hsp70 does not bind directly to NudC, we

found that Hsp70 can still bind to Hsp40 when in complex with NudC (Figure 3A). Notably, this interaction was ATP-dependent, suggesting that Hsp70 binds to Hsp40 via the J-domain (Figure 3A). To determine which region of NudC is responsible for Hsp40 binding, an excess of unlabeled NudC fragment (Figure 2A) was added to a preformed complex between NudC* and Hsp40, and the displacement was followed by aUC (Figure 3B). All constructs containing the N-terminal region of NudC (aa 1–141, 1–274, 1–331) released NudC* from Hsp40, whereas the C-terminal fragments (aa 158–274, 158–331) had no effect (Figure 3B). A monomeric construct lacking the helices α1 and α2 (NudC$^{50-331}$) was also able to displace NudC* from Hsp40, suggesting that the binding motif for Hsp40 is located within the α3-α4 region (aa 50–141) and that the helices α1 and α2 are not required for the interaction.

To study the binding of NudC to Hsp40s in more detail and with a native binding partner, NudC was tested with human DNAJB1. NMR spectra of ^{15}N-labeled dimeric NudC$^{1-141}$ show an overall line-broadening and signal-intensity reduction in the presence of the human Hsp40 protein DNAJB1 (Figures 3C and S7A), confirming the interaction. The strongest spectral changes were observed for NudC helix α4 (residues Q103 to E126) (Figure S7A). Titrations using ^{13}CH$_3$-labeled Hsp40/DNAJB1 (comprising the CTDs and the dimerization region (DD)) and unlabeled NudC (Figures 3D and S7B) revealed CSPs mainly in the CTD-I and part of the DNAJB1 G/F linker by NudC binding. No perturbations were observed in the J-domain, the CTD-II region, or the dimerization domain (Figures 3D and S7B). Titration of NudC$^{1-141}$ to the ^{15}N-labeled Hsp40 class A yeast homolog Ydj1 yielded similar results, suggesting that the binding of NudC is conserved between class A and class B Hsp40s and between the human and yeast system (Figures S7C and S10B).

Based on the mapping of the NudC/Hsp40 interacting regions by NMR, we could crystallize a minimal complex composed of Hsp40/DNAJB1^{CTDs} and NudC$^{100-141}$. The structure of the DNAJB1^{CTDs} dimer bound to two NudC$^{100-141}$ fragments was determined to 2.5 Å resolution (Figure 3E). The binding interface in NudC comprises a β-strand (residues 103–106) and the helix α4 (residues 109–125), which interact with the CTD-I of DNAJB1 (Figures 3E–3H). Interestingly, the residues 103–106 are unstructured in NudC alone (Figure S2D) and adopt a β-strand

Figure 2. NudC binds Hsp90 with its CS domain

(A) Domain constructs of NudC. The schematic domain architecture of NudC and truncations were used.

(B) The NudC-CS domain interacts with Hsp90. A competition aUC experiment was performed in which the complex formation between labeled NudC* and Hsp90α was analyzed in the presence of the indicated NudC fragments that were added in 20-fold molar excess. The measurement was performed in the absence of nucleotides. The quantification represents means ± SD determined from three independent experiments. Statistical significance was determined by student-t test (n.s. p ≥ 0.05; * p < 0.05, ** p < 0.01, *** p < 0.001) [NudC*: 500 nM, Hsp90α: 4 μM, NudC fragments: 10 μM].

(C) Chemical shift perturbations and intensity changes of Hsp90 ^{13}CH$_3$-IM resonances upon the addition of unlabeled NudC. Bar graphs showing CSPs (top graph) or intensity changes (bottom graph) of Hsp90 labeled residues along the sequence. Residues without CSP or change of intensity are shown in gray, residues with significant CSP (>0.02) are shown in red, and residues with significant intensity change (<0.45) but without significant CSP are shown in blue.

(D) Hsp90 ^{13}CH$_3$-IM-labeled ^{1}H-^{13}C methyl-TROSY spectrum. The overlay of the ^{1}H-^{13}C HMQC spectrum of isoleucine region of Hsp90 alone (black) or after addition of unlabeled NudC (red).

(E) Representation of significantly perturbated residues on Hsp90 structure. Illustration of the structure of Hsp90 (PDB: 5FWK). Assigned residues are shown in spheres; color-coding follows the one used in (C).

(F) Representation of significantly perturbated residues on the Hsp90^{MD} after the addition of NudC$^{158-274}$ to ^{15}N Hsp90^{MD}, as shown in Figure S4. Surface representation of the structure of Hsp90^{MD} extracted from PDB: 5FWK. CSPs are shown in red.

(G) Representation of significantly perturbated residues on NudC^{CS} after the addition of the Hsp90^{MD} to ^{15}N-NudC$^{158-274}$. Surface representation of the structure of NudC$^{158-274}$ (PDB: 3QOR). CSPs are shown in blue.
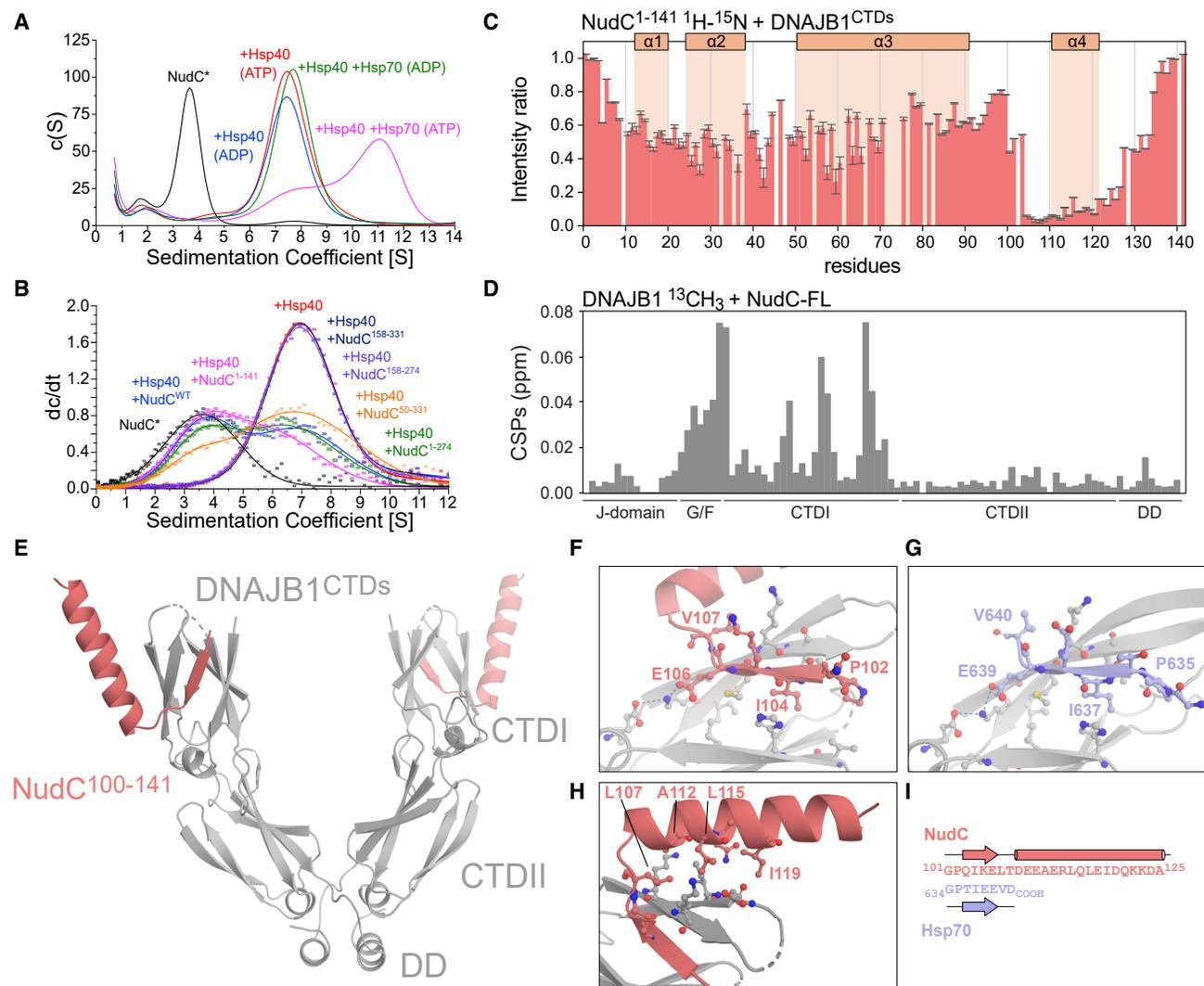
Figure 3. NudC helix α4 interacts with Hsp40

(A) NudC forms a high-molecular-weight complex with the Hsp40/Hsp70 system. The sedimentation coefficient distribution of an aUC experiment with labeled NudC*, Hsp40, and Hsp70 is shown. The experiment was performed in the presence of 2 mM ADP or ATP as indicated [NudC*: 500 nM, Hsp40 (Ydj1): 4 μM, Hsp70: 3 μM].

(B) The NudC helix α4 domain interacts with Hsp40. The sedimentation trace of a competition aUC experiment is shown. The complex formation between labeled NudC* and Hsp40 was analyzed in the presence of a 20-fold molar excess of the unlabeled depicted NudC fragments. The experiments were conducted in the absence of nucleotides [NudC*: 500 nM, Hsp40 (Ydj1): 4 μM, NudC fragments: 10 μM].

(C) Intensity changes in ^{1}H-^{15}N resonances of NudC$^{1-141}$ upon the addition of DNAJB1^{CTDs}.Topology is indicated at the top of the graph. Error bars are calculated from the S/N ratio of each peak in both spectra.

(D) Chemical shift perturbations of DNAJB1 ^{13}CH$_3$ resonances upon the addition of unlabeled NudC. Bar graphs showing CSPs on labeled DNAJB1 residues.

(E) Overall structure of the complex between DNAJB1^{CTDs} and NudC$^{100-141}$. DNAJB1^{CTDs} is shown in gray, and NudC$^{100-141}$ is shown in red.

(F) Detail of the strand binding of NudC$^{100-141}$ to DNAJB1^{CTDs}. Relevant residues are shown in sticks. Conserved residues between NudC and Hsp70 are labeled.

(G) Detail of the strand binding of Hsp70 to DNAJB1^{CTDs}. Relevant residues are shown in sticks. Conserved residues between NudC and Hsp70 are labeled. Structure from PDB: 3AGX.

(H) Detail of the helix α4 binding of NudC$^{100-141}$ to DNAJB1^{CTDs}. Relevant residues are shown in sticks. Residues of NudC involved in the interaction with DNAJB1 are labeled.

(I) Alignment of the C-terminal tail of Hsp70 (blue) with the Hsp40-binding site of NudC (red).

conformation only after binding to DNAJB1, thereby extending the β-sheet of the CTD-I. The interaction involves a hydrophobic groove of the CTD-I that has previously been shown to interact both with substrates (Jiang et al., 2019) and the C-terminal motif of Hsp70 (Figure 3I) (Suzuki et al., 2010). In fact, key residues that mediate the interaction (I104, E106 in NudC) are identical with those in Hsp70 (Figures 3F and 3G). However, distinct from the Hsp70 interaction, NudC binding is complemented by additional
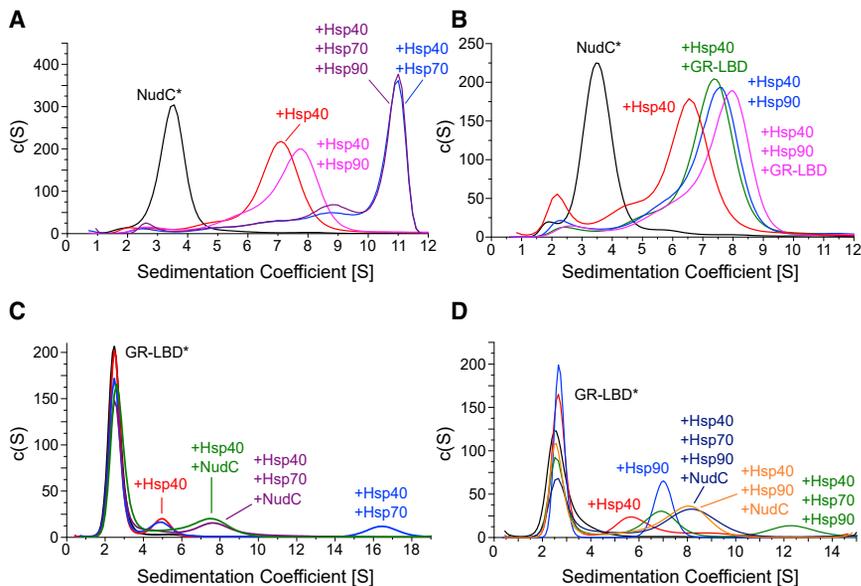
Figure 4. NudC mediates client transfer to Hsp90

(A) NudC does not bridge Hsp70 and Hsp90. The sedimentation coefficient distribution of an aUC experiment is shown in which labeled NudC* was mixed with the depicted components in the presence of 2 mM ATP. No simultaneous binding of Hsp70 and Hsp90 to NudC:Hsp40 could be observed [Hsp90α: 4 μM, Hsp40 (Ydj1): 4 μM, Hsp70: 3 μM].

(B) NudC forms contacts with Hsp40 and Hsp90 in the presence of a client. The complex formation between the labeled NudC*,Hsp40, and Hsp90α was analyzed by aUC in the presence of GR-LBD. The sedimentation coefficient distribution is depicted. Complex formation was monitored in the presence of 2 mM ATP [NudC*: 500 nM, Hsp40 (Ydj1): 4 μM, Hsp90α: 4 μM, GR-LBD: 4 μM].

(C) NudC disrupts the Hsp40:Hsp70:client complex. The sedimentation coefficient distribution of an aUC experiment is shown. The disruption of the GR-LBD*:Hsp40:Hsp70 by the addition of NudC is shown. The experiment was performed in the presence of 2 mM ATP [GR-LBD*: 500 nM, Hsp40 (Ydj1): 4 μM, Hsp70: 3 μM, NudC: 6 μM].

(D) NudC facilitates client transfer to Hsp90. The sedimentation coefficient distribution of an aUC experiment is depicted. The complex formation between labeled GR-LBD*, Hsp40, and Hsp70 is shown in the presence of NudC and Hsp90, leading the formation of a GR-LBD*:Hsp40:NudC:Hsp90 complex. The experiment was performed in the presence of 2 mM ATP [GR-LBD*: 500 nM, Hsp40 (Ydj1): 4 μM, Hsp70: 3 μM, Hsp90α: 4 μM, NudC: 10 μM].

conserved hydrophobic residues in helix α4 (Figures 3E and S7D), thereby creating multiple contacts with aliphatic sidechains at the surface of the CTD-I (Figure 3H). To validate this extended binding interface, an I104A substitution within the NudC β-strand and a L107A substitution in the helix α4 were introduced. The mutations disrupted the interaction between NudC and yeast Hsp40 (Ydj1), suggesting that the interaction mechanism of NudC with Hsp40s is conserved (Figure S7E). In summary, the interaction of NudC with the Hsp40 CTD-I resembles that of Hsp40 CTD-I with Hsp70 but shows unique extended hydrophobic interactions.

NudC connects Hsp40 to Hsp90

The unique molecular interactions of NudC suggested that it may bridge the Hsp40/Hsp70 and Hsp90 systems. To test this, we used aUC to study different combinations of NudC binding partners (Figure 4A; Table S1). Interestingly, in addition to the complexes described above, a NudC*:Hsp40:Hsp90 complex was observed, in perfect agreement with our findings that NudC binds Hsp40 and Hsp90 via two independent binding sites. NMR titrations using ^{13}C-Ile labeled NudC with unlabeled Hsp90 and Hsp40 (DNAJB1) (Figures S8A–S8E) showed that in presence of both proteins, changes of intensity are observed for residues in the CS domain (Figures S8D and S8E) and Hsp40-binding motif (Figures S8C and S8E). Thus, the previously determined binding modes of NudC with Hsp40 and Hsp90 are preserved in the ternary complex. We used the Hsp90^{MD}/NudC^{CS} docking model (Figure S5) and the structure of NudC$^{100-141}$ with DNAJB1^{CTDs} (Figure 3E) to generate a model of the Hsp40:Hsp90:NudC complex (Figure S8F). The model of the ternary complex shows that NudC can simultaneously connect Hsp40 and Hsp90 in a 2:2:2 stoichiometry without steric hindrance.

NudC is involved in client transfer from Hsp40/Hsp70 to Hsp90

Because previous work suggested that NudC may have a similar interaction profile as Hop (Taipale et al., 2014), we hypothesized that NudC may have partially overlapping functions with Hop in client recruitment. No quaternary NudC*:Hsp40:Hsp70:Hsp90 complex could be detected by aUC (Figures 4A and S9A). This indicates that NudC cannot connect the Hsp70 system to Hsp90 and that Hsp70 and Hsp90 sterically compete for binding to this complex or induce conformations in the NudC:Hsp40 complex that are incompatible for simultaneous binding of the large Hsp70 and Hsp90 chaperones. Next, we investigated how the client handover from Hsp40/70 to Hsp90 is modulated by NudC (Figures 4B and 4D; Table S1). We used the ligand binding domain of GR (GR-LBD) as a stringent client that is transferred from Hsp40/Hsp70 to Hsp90 with the help of Hop (Chen and Smith, 1998; Kirschke et al., 2014; Lorenz et al., 2014).

Our aUC analysis revealed that NudC binds the GR-LBD directly with a weak affinity of approximately 10 μM (Figure S9B). NMR using ^{15}N and ^{13}CH$_3$-labeled NudC samples revealed that GR-LBD directly interacts with the C-terminal helix α6 from NudC (Figure S9) and that the interaction is conserved even in presence of Hsp40.

We then used low GR-LBD concentrations at which the direct binding to NudC is negligible (Figure S9J). aUC analysis showed that the GR-LBD and NudC* can simultaneously interact with Hsp90 (Figures 4B and 4D). In addition, the ternary NudC:Hsp40:GR-LBD complex could also be formed, in line with the view that clients and NudC associate with different regions of Hsp40s (Figures 4B, 4C, and S9J). NMR spectroscopy confirmed that the GR-LBD and NudC have nonoverlapping binding sites on Hsp40 (Figures S7C and S10). Furthermore, the NudC*:Hsp40:GR-LBD module could also bind Hsp90 (Figure 4B),

suggesting that NudC may recruit Hsp40-bound clients directly to Hsp90, either bypassing Hsp70 completely or following the Hsp70 release. Importantly, our aUC data showed the recruitment of Hsp90 to a preformed NudC*:Hsp40:GR-LBD complex, indicating that the presence of Hsp70 chaperone is not required (Figure S8K). When Hsp70 was incubated with the GR-LBD*:Hsp40 complex, a shift in the sedimentation coefficient was observed, from approximately 5S to 16.5S, suggesting that several Hsp70 molecules bind simultaneously—most likely to the client protein (Figures 4C and S9L; Table S1). Surprisingly, when NudC was also present, these high-molecular-weight species disappeared, indicating that NudC inhibits the assembly or induces the disassembly of the GR-LBD*:Hsp40:Hsp70 complex. Furthermore, a species sedimenting at approximately 7.5S was detected, which is identical to the sedimentation coefficient observed for the GR-LBD*:Hsp40:NudC complex (Figure 4C). To confirm that the observed 7.5S peak is indeed the GR-LBD*:Hsp40:NudC complex, we repeated the experiment with NudC[1–141], which binds Hsp40 but is approximately 20 kDa smaller than NudC[WT]. The presence of NudC[1–141] together with GR-LBD*, Hsp40, and Hsp70 resulted in the emergence of a smaller complex (6S as compared to 7.5 S with NudC[WT]) (Figure S9M; Table S1), confirming the formation of a GR-LBD*:Hsp40:NudC[1–141] complex that lacks Hsp70. Additionally, this result indicates that it is not the direct interaction of NudC and GR-LBD that causes the dissociation of Hsp70 because the NudC[1–141] fragment lacks the GR-LBD interaction site. To further test whether the dissociation of Hsp70 is because of the competition between Hsp70 and NudC for the same binding site on Hsp40 CTD-I, we repeated this experiment with NudC[I104A/L107A], which cannot bind Hsp40 (Figure S9N). Indeed, this NudC mutant could not dissociate the large GR-LBD:Hsp40:Hsp70 complex, providing evidence that the interaction of NudC with Hsp40 is required for this effect (Figure S9N). Furthermore, the addition of NudC to preformed GR-LBD*:Hsp40:Hsp70 mixture showed a clear dissociation of this complex, as observed by aUC (Figure S9O). Together, these results suggest that NudC may either recruit Hsp40-bound clients to Hsp90, bypassing Hsp70, or strip Hsp70 from the Hsp40:Hsp70:client assemblies. Both scenarios yield a NudC:Hsp40:client complex. We then tested the effect of NudC when it was in a sample containing the GR-LBD*:Hsp40:Hsp70 complex in the presence of Hsp90 but without Hop. The presence of Hsp90 led to a slightly reduced size of the GR-LBD*:Hsp40:Hsp70 complex. Importantly, we observed that the presence of NudC led to the formation of an 8S species that matched the sedimentation coefficient of the GR-LBD*:Hsp40:Hsp90:NudC complex (Figure 4D).

In summary, these data show that NudC depletes Hsp70 from the Hsp40:Hsp70:client complex but retains the client, allowing the transfer of the resulting NudC:Hsp40:client complex to Hsp90. This suggests that Hsp40-bound clients can be recruited to Hsp90 via NudC without any need for Hsp70 or Hop.

NudC facilitates client release from the Hsp40/70 system and the transfer to Hsp90

If our hypothesis of a productive client transfer from Hsp40/Hsp70 to Hsp90 by NudC is correct, NudC should have an influence on the ability of the GR-LBD to bind hormones (Chen and

Smith, 1998; Dittmar et al., 1996; Johnson et al., 1998; Kirschke et al., 2014; Lorenz et al., 2014). Previous work reveals that hormones dissociate from GR-LBD when bound to Hsp40/Hsp70 in the presence of ATP and that releasing the GR-LBD from the Hsp40/Hsp70 deadlock restores its hormone binding capacity (Kirschke et al., 2014). When we incubated the GR-LBD with Hsp40/Hsp70/ATP, the equilibrium binding values to dexamethasone fluorescein (F-Dex) were markedly reduced (Figures 5 and S11A). After the addition of Hop, Hsp90, or both, a moderate increase in F-Dex binding was observed. When NudC alone was added to GR-LBD/Hsp40/Hsp70, we detected a strong increase in hormone binding, suggesting that NudC releases GR-LBD from Hsp40/Hsp70. Furthermore, when present in combination with Hsp90 to GR-LBD/Hsp40/Hsp70, NudC increased hormone binding back to the level of the native GR-LBD. Taken together, these results show that NudC releases GR-LBD from Hsp70/40 such that it partially recovers its activity. In the additional presence of Hsp90, NudC allows the complete regain of GR-functionality in an ATP-dependent reaction.

Next, we were interested to test whether the direct interaction of NudC with the GR-LBD or the interaction of NudC with Hsp40 was responsible for the observed effect on hormone binding efficiency (Figures 5D and S11B). The presence of NudC[WT] and NudC[1–274] had a similar positive effect on hormone binding, indicating that the direct interaction of NudC with GR-LBD has only a small effect. In agreement with this finding, the presence of NudC[158–274] or and NudC[158–331] could not rescue hormone binding, suggesting that the interaction with Hsp40 is required for this effect.

To further dissect the transfer process of GR-LBD to Hsp90, we performed timed-addition experiments in which apo-GR-LBD was first incubated with F-Dex. Then, Hsp40, Hsp70, and ATP were added to release F-Dex, and, finally, hormone binding recovery was induced by the addition of NudC, Hsp90, or NudC with Hsp90 (Figures 5E and 5F). As a control, we confirmed that the addition of Hsp40 and ATP in the absence of Hsp70 did not lead to the release of the hormone (Figure S12A). Although the addition of Hsp90 had a small effect on hormone binding recovery, the timed addition of NudC led to a significant increase in hormone binding (Figures 5E and 5F). By contrast, the addition of NudC[I104A/L107A], which cannot bind Hsp40, did not lead to the recovery of hormone binding (Figure S12B). The addition of NudC together with Hsp90 led to a strong synergistic effect on hormone binding recovery, reaching levels similar to that of GR alone before the incubation with Hsp40, Hsp70, and ATP (Figure 5F). These results show that NudC inhibits the binding of Hsp70 to Hsp40:GR-LBD and recruits this complex to Hsp90.

The Hsp90 co-chaperone p23 has been found to be important for GR-LBD maturation (Biebl et al., 2021; López et al., 2021; Lorenz et al., 2014; Sahasrabudhe et al., 2017). Importantly, NudC with Hsp90 led to hormone binding efficiencies reaching the native state of the GR-LBD, which could not be further promoted by p23 (Figure S12C). By contrast, Hop with Hsp90 only partially recovered hormone binding and p23 was required for a full hormone binding recovery (Figures 5C and S12D). Importantly, this indicates that p23 is important for the Hop-mediated maturation of the GR-LBD but is dispensable for the maturation of the GR-LBD via the NudC pathway.
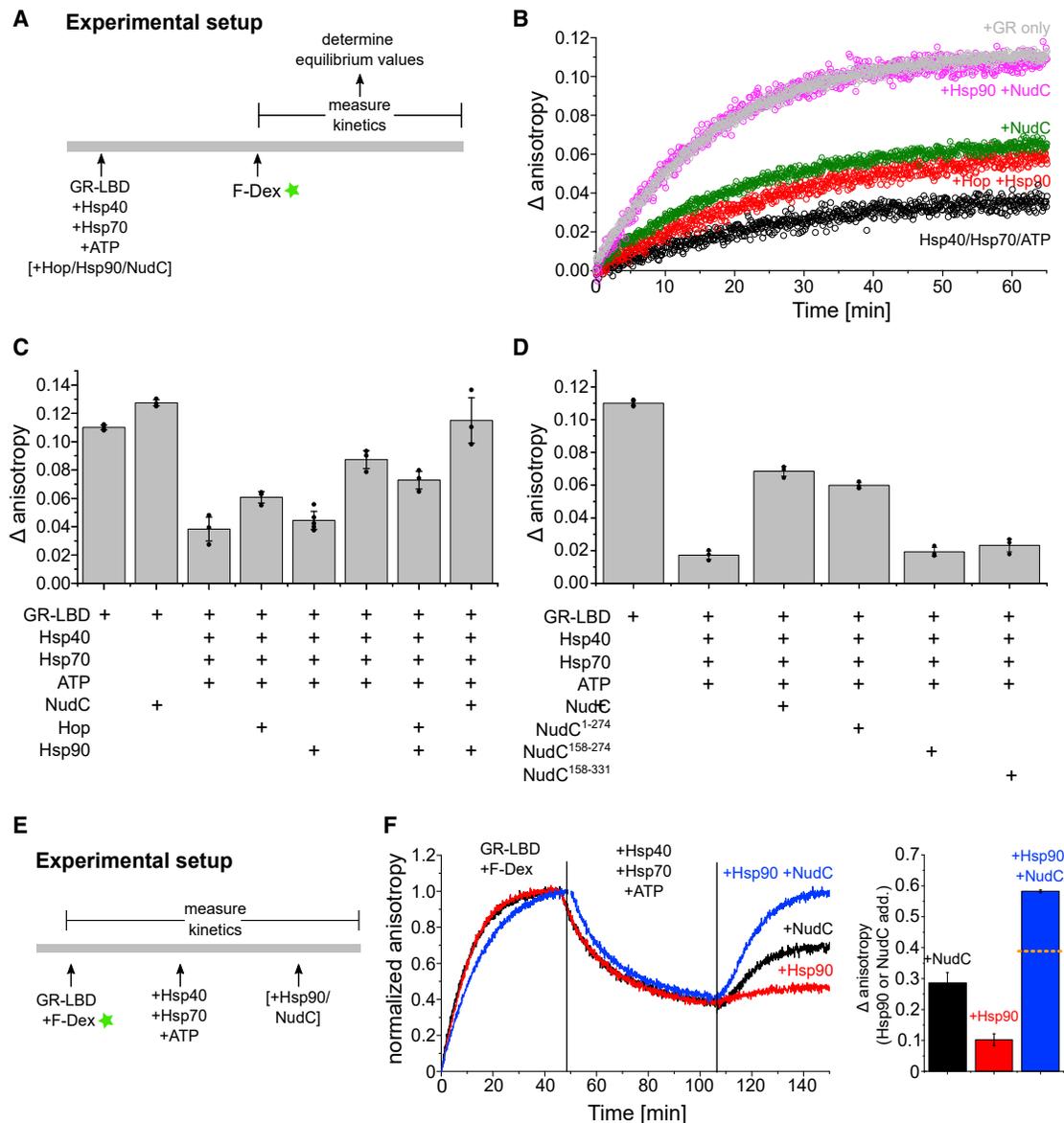
Figure 5. NudC promotes GR maturation *in vitro*

(A) Assay setup to follow hormone binding to the GR-LBD. The schematic workflow of fluorescence anisotropy experiments that allow the investigation of hormone binding to the GR-LBD is shown. The apo-GR-LBD was pre-incubated with Hsp40 (Ydj1, 2 μM), Hsp70 (12 μM), ATP (5 mM) and chaperones (12 μM) for 60 min. After the addition of fluorescein-dexamethasone (F-Dex, 100 nM) to start the reaction, the fluorescence anisotropy was measured to determine equilibrium values.

(B) NudC promotes hormone binding to the GR-LBD. Representative fluorescence anisotropy traces that represent the binding of F-Dex to the GR-LBD over time are shown. The initial anisotropy value immediately after the addition of F-Dex was set to 0. All experiments were performed in triplicates as shown in (C).

(C) NudC increases the equilibrium binding efficiency of hormone to the GR-LBD. The equilibrium fluorescence anisotropy changes ("end points") are depicted for reactions with the shown components. Representative traces are depicted in (B). All experiments were performed in triplicates and the means and standard deviations are depicted. The individual traces are shown in Figure S11A.

(D) NudC increases the hormone binding efficiency of GR-LBD due to the interaction with Hsp40. The equilibrium fluorescence anisotropy changes ("end points") are shown for reactions with the shown proteins. The measurements were performed in triplicates. The individual traces are shown in Figure S11B.

(E) Experimental setup for timed-addition hormone binding recovery to the GR-LBD. Apo-GR-LBD (1 μM) was mixed with 100 nM F-Dex and the binding of hormone was recorded by measuring the change in fluorescence anisotropy as a function of time. Then, Hsp40 (1.83 μM), Hsp70 (11.1 μM), and ATP (4.6 mM) were added to release hormone. In the last step, NudC (16.5 μM), Hsp90 (13.5 μM), or both proteins were added to the sample.

(F) NudC frees the GR-LBD from Hsp70 and promotes hormone binding synergistically with Hsp90. (Left) The binding of F-Dex to the GR-LBD was monitored by measuring the fluorescence anisotropy. The indicated proteins were added as depicted. The anisotropy values were normalized to the maximum anisotropy reached when GR-LBD was incubated with F-Dex. The immediate y-offset caused by the addition of NudC or Hsp90 was subtracted (see Figure S12). (Right) The anisotropy change after the addition of NudC, Hsp90, or NudC with Hsp90 was quantified. The dotted line represents the expected anisotropy change assuming an additive effect of NudC and Hsp90.

To investigate whether the function of NudC identified for the GR-LBD reflects a more general mechanism for NudC in client activation, we measured the effect of NudC on the folding of another well-studied Hsp90 client, p53 (Blagosklonny et al., 1996; Hagn et al., 2011; Müller et al., 2004; Rüdiger et al., 2002; Sepehrnia et al., 1996). Here, we used single-pair FRET (spFRET) to follow the chaperone-mediated folding of the p53-DNA-binding domain (p53-DBD), a client we have studied previously (Dahiya et al., 2019). Similar to what we observed for GR-LBD, NudC increased the kinetics and efficiency of the p53 folding (Figure S13).

We also followed the folding of p53 by monitoring its aggregation in the presence of NudC, Hsp90, or both. The addition of NudC to the p53-DBD/Hsp40/Hsp70 complex led to release of the p53-DBD, resulting in the aggregation of p53-DBD at elevated temperature (Figure S14). The addition of Hsp90 alone did not release Hsp70, and, hence, no p53-DBD aggregation was observed (Figure S14) (Dahiya et al., 2019). By contrast, the simultaneous addition of NudC and Hsp90 almost completely suppressed the aggregation (Figure S14). These results suggest that NudC aids in recruiting p53-DBD:Hsp40 to Hsp90 and that the positive effect of NudC on the maturation of stringent Hsp90 clients is not client-specific.

DISCUSSION

For many Hsp90 clients, the sequential action of the Hsp40/Hsp70 system and Hsp90 is required to ensure their proper folding and maturation. Although chaperones are generally perceived as promoters of folding, they can also trap substrates in a largely folded but inactive state. This behavior has been observed for the activity of Hsp70 on p53 (Boysen et al., 2019; Dahiya et al., 2019), GR (Kirschke et al., 2014), and luciferase (Morán Luengo et al., 2018). Hop and Hsp90 can promote the release of substrates from this folding trap and feed the proteins into a productive folding pathway. The co-chaperone Hop serves as a physical bridge between the two chaperone systems, binding to Hsp70 and Hsp90, thus facilitating the transfer of clients from Hsp40/70 to Hsp90 (Chen and Smith, 1998; Johnson et al., 1998; Röhl et al., 2015; Schmid et al., 2012; Smith et al., 1993; Wegele et al., 2006). Whether additional co-chaperones affect this process of central importance has remained unknown. Although some clients may require the transfer from Hsp40/Hsp70 to Hsp90 only once to reach their native folds, other clients may require repeated cycling between Hsp40/Hsp70 and Hsp90 for their activity (Boczek et al., 2015; Mayer and Le Breton, 2015; Xu et al., 1999). Hence, the existence of multiple factors facilitating the transfer between these two chaperone systems would be biologically favorable.

Here, we show that NudC is a co-chaperone that opens a unique pathway to recruit clients to Hsp90, connecting two major chaperone systems in the cell (Figure 6). Consistent with this, both have similar cellular concentrations (Finka and Goloubinoff, 2013). Clients are first bound by Hsp40. Although Hsp40 stabilizes partially unfolded conformations, the binding of Hsp70 may be required for some clients or client conformations to further unfold the client. Notably, recent studies suggest that Hsp40s bind clients tightly whereas Hsp70 undergoes cycles

of binding and unbinding (Faust et al., 2020; Wentink et al., 2020). NudC can either directly associate with Hsp40-bound clients or prevent continuous rebinding of Hsp70 by competing with Hsp70 for Hsp40-binding, and the resulting NudC:Hsp40:client complex is recruited to Hsp90 via NudC. The direct interaction of NudC with the client further promotes the formation of the NudC:Hsp40:client complex for the GR-LBD. The Hsp40 bound to the client in this complex may be important to stabilize the partially unfolded regions. After the recruitment of the NudC:Hsp40:client complex to Hsp90, Hsp90 forms contacts with the client that will ultimately result in the release of the mature client, Hsp40, and NudC. Hence, NudC provides a shortcut for client recruitment to Hsp90, bypassing the canonical Hop pathway. Interestingly, while p23 has been found to be important for the maturation of clients in the Hop-mediated maturation pathway, it seems dispensable in the NudC-mediated pathway. Intriguingly, the NudC recruiting pathway creates multiple routes for client recruitment due to the interaction of NudC with different Hsp40 classes. Notably, depending on whether Hsp40 is still bound to client in the Hsp90/Hop/Hsp70/client complex, NudC can also promote the disassembly of this complex and accelerate client transfer to Hsp90. The existence of partially parallel pathways may be beneficial to adapt to the different conformational needs of a client.

Although NudC and Hop both promote client transfer, their mode of action is strikingly different. The major difference is their effect on the Hsp70/Hsp40/client complex. Hop binds to Hsp70, whereas NudC interacts with Hsp40. Furthermore, the binding of NudC to Hsp40 blocks the binding of Hsp70. How the binding of Hop to Hsp70 affects the Hsp40 binding is not entirely clear, but Hop may release Hsp40 from the complex (Cintron and Toft, 2006; Dittmar et al., 1998; Hernández et al., 2002). Hop primarily interacts with the C terminus of Hsp90, with secondary contacts along the Hsp90^{MD} and Hsp90^{NTD} (Prodromou et al., 1999; Richter et al., 2003; Schmid et al., 2012; Wang et al., 2020). By contrast, the NudC interaction site is primarily mediated by the Hsp90^{MD} and the binding seemed to be independent of the Hsp90 conformation. Additionally, Hop binds to Hsp90 as a monomer, whereas NudC interacts with Hsp90 as a dimer. The different interaction of NudC also results in different effects on Hsp90. Although Hop inhibits the Hsp90 ATPase in a noncompetitive manner, NudC did not have an effect. This opposes previous findings (Zhu et al., 2010) but matches the nucleotide-independent Hsp90 binding of NudC. The discrepancy between earlier studies and our study regarding the Hsp90 ATPase regulation by NudC may be due to distinct experimental setups, including the type of ATPase assay, buffer conditions, and protein concentrations. For the release of Hop from Hsp90, the Hsp90 co-chaperones Aha1 and p23 as well as ATP binding are important (Li et al., 2013; Xu et al., 2019). Based on the available Hsp90:client structures in which the client occupies both faces of the Hsp90 MD (Lorenz et al., 2014; Verba et al., 2016; Wang et al., 2020), stable binding of the client to Hsp90 could compete with the binding of NudC and promote its release from Hsp90.

The release of clients from Hsp70 by NudC can, in principle, entail their productive folding also in the absence of Hsp90. Because the concentration of Hsp90 is approximately 15 times
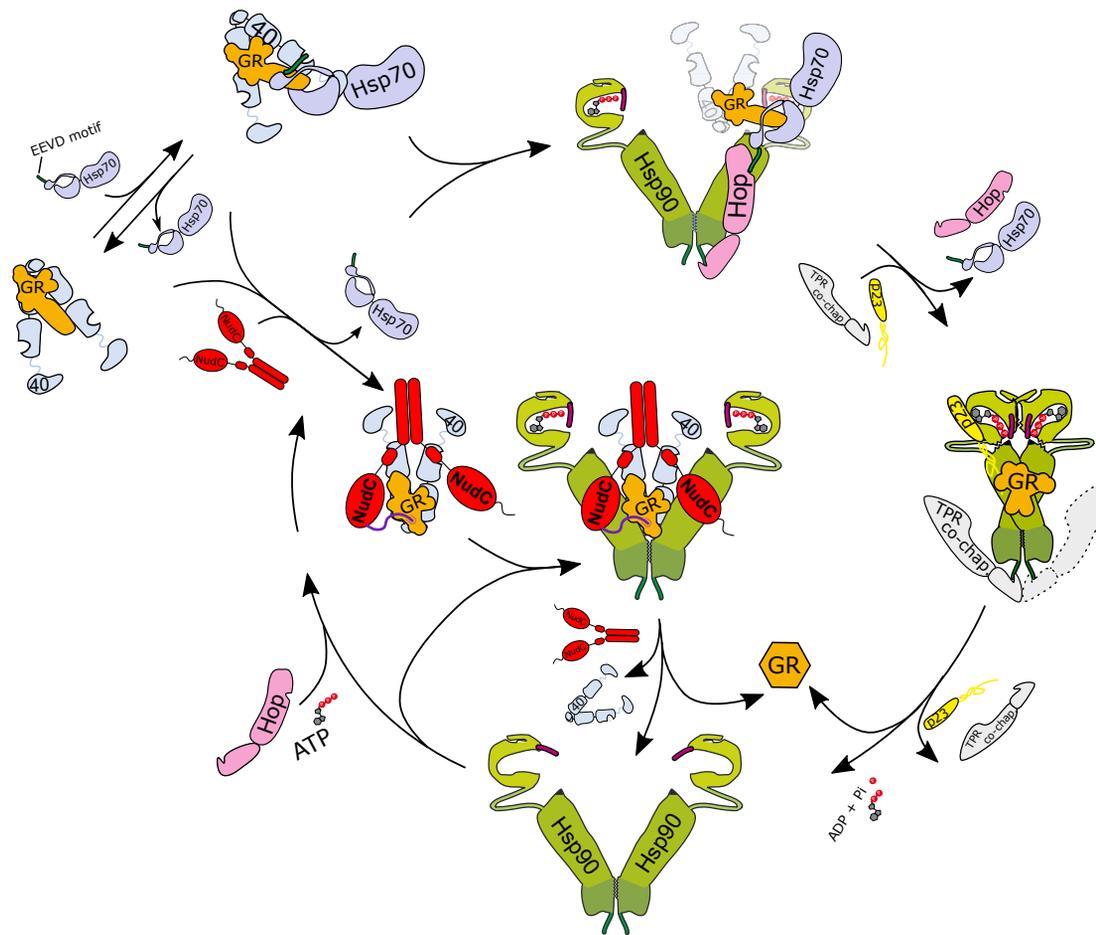
Figure 6. Schematic integration of NudC into the client maturation process

A schematic model of the NudC function is shown with the GR-LBD as a model client. Clients are initially bound by Hsp40. Binding of Hsp70 may be required for some conformations of a client and leads to a (partial) unfolding of the substrate priming it for the interaction with Hsp90. In the canonical pathway, clients are transferred to Hsp90 with the help of Hop. The reduced binding of Hsp40 to the client after Hsp70 and Hop binding is indicated by reduced opacity. NudC promotes client recruitment to Hsp90 by recruiting the Hsp40-bound clients to Hsp90 bypassing Hop. In these complexes, NudC forms a direct interaction with the GR-LBD via its terminal α-helix. Notably, NudC binding to Hsp40:Hsp70-bound clients will lead to the release of Hsp70. Although p23 seems to be important in the Hop-mediated maturation pathway, it is dispensable in the NudC-mediated maturation of clients.

higher than that of NudC in the cell, few NudC molecules will exist in the unbound state. Notably, Hsp70 recognition motifs are frequent in proteins and a nonnative protein may be coated by several Hsp40 and Hsp70 proteins (Rüdiger et al., 1997). The random release of individual Hsp70s by free NudC may be beneficial to increase the Hsp70 binding fidelity to the thermodynamically most unstable areas of a substrate (Rosenzweig et al., 2019). That way, the action of NudC may conserve energy by reducing the number of unproductive binding/unbinding cycles of Hsp70. Notably, the exposure of these regions may change while the protein samples different near-native conformations. Thus, NudC could also enhance the dynamics of Hsp40/Hsp70 association to allow folding progression. However, our results show that handover to Hsp90 increases the productive folding.

In addition to its association with Hsp70 and Hsp90 complexes (Taipale et al., 2014), NudC has been shown to affect processes such as cytokinesis, nuclear migration, macrophage

differentiation, platelet production, and ciliogenesis via the interaction with different regulators such as Plk1, Lis1, PAF-AH (I), Mp1, and cofilin 1 (Fu et al., 2016). Whether all these processes depend on the interaction of NudC with Hsp90 remains to be seen as for other Hsp90 co-chaperones also, independent functions have been proposed (Bose et al., 1996; Echeverría et al., 2011; Echtenkamp et al., 2016; Freeman and Morimoto, 1996). This idea is supported by the structural homology of NudC with the co-chaperone p23, which acts in different contexts (Biebl et al., 2021; Bose et al., 1996; Freeman and Morimoto, 1996).

Our findings show that NudC is a factor that releases Hsp70 from complexes with Hsp40 and client by binding to Hsp40. Thus, NudC can be viewed as a direct regulator of Hsp40 functioning as a "co-chaperone of a co-chaperone." In addition, NudC acts as a recruiter of Hsp40-bound clients to Hsp90, hence additionally functioning as an Hsp90 co-chaperone. Together,

NudC is a unique co-chaperone with bipartite function, regulating the Hsp70 and the Hsp90 systems to ease the client transfer from Hsp70 to Hsp90 and, thus, improve the client folding.

Limitations of the study

Due to the transient nature of the complexes involving NudC and client, a detailed structural analysis was not possible. Also, it is technically not possible yet to follow the changes of the conformation of the client protein in the different complexes in detail *in vitro* and *in vivo*. In AUC coupled to fluorescence detection, the signal for complexes involved multiple components and does not always unambiguously report on their composition, which requires the use of orthogonal methods. Although we see the product of client transfer, we are lacking methods that would allow us to monitor the actual transfer reaction *in vivo* and *in vivo* without manipulating the system to some extent. Finally, it remains to be seen whether NudC exhibits client specificity or whether it is largely promiscuous in its interaction.

STAR★METHODS

Detailed methods are provided in the online version of this paper and include the following:

- KEY RESOURCES TABLE
- RESOURCE AVAILABILITY
  - Lead contact
  - Material availability
  - Data and code availability
- EXPERIMENTAL MODEL AND SUBJECT DETAILS
  - Cell lines and plasmids
- METHOD DETAILS
  - CRISPRi library design
  - CRISPRi screening for modulators
  - *In vivo* GR activity measurement
  - *In vivo* viability analysis of knockdown strains
  - RT-qPCR
  - Western Blot
  - Protein expression and purification
  - NMR
  - Calculation of structural models
  - Crystallography
  - Analytical Ultracentrifugation
  - Single-pair FRET experiments
  - p53-DBD Aggregation Assay
  - Fluorescence Anisotropy
  - Fluorescence Polarization
  - SEC-MALS
  - ATPase assay
- QUANTIFICATION AND STATISTICAL ANALYSIS

SUPPLEMENTAL INFORMATION

Supplemental information can be found online at https://doi.org/10.1016/j.molcel.2021.12.031.

REFERENCES

Ali, J.A., Jackson, A.P., Howells, A.J., and Maxwell, A. (1993). The 43-kilodalton N-terminal fragment of the DNA gyrase B protein hydrolyzes ATP and binds coumarin drugs. Biochemistry *32*, 2717–2724.

Ali, M.M., Roe, S.M., Vaughan, C.K., Meyer, P., Panaretou, B., Piper, P.W., Prodromou, C., and Pearl, L.H. (2006). Crystal structure of an Hsp90-nucleotide-p23/Sba1 closed chaperone complex. Nature *440*, 1013–1017.

Aron, R., Lopez, N., Walter, W., Craig, E.A., and Johnson, J. (2005). In vivo bipartite interaction between the Hsp40 Sis1 and Hsp70 in Saccharomyces cerevisiae. Genetics *169*, 1873–1882.

Balchin, D., Hayer-Hartl, M., and Hartl, F.U. (2016). In vivo aspects of protein folding and quality control. Science *353*, aac4354.

Battiste, J.L., and Wagner, G. (2000). Utilization of site-directed spin labeling and high-resolution heteronuclear nuclear magnetic resonance for global fold determination of large proteins with limited nuclear overhauser effect data. Biochemistry *39*, 5355–5365.

Bernadó, P., Mylonas, E., Petoukhov, M.V., Blackledge, M., and Svergun, D.I. (2007). Structural characterization of flexible proteins using small-angle X-ray scattering. J. Am. Chem. Soc. *129*, 5656–5664.

Bhattacharya, K., Weidenauer, L., Luengo, T.M., Pieters, E.C., Echeverría, P.C., Bernasconi, L., Wider, D., Sadian, Y., Koopman, M.B., Villemin, M., et al. (2020). The Hsp70-Hsp90 co-chaperone Hop/Stip1 shifts the proteostatic balance from folding towards degradation. Nat. Commun. *11*, 5975.

Biebl, M.M., and Buchner, J. (2019). Structure, function, and regulation of the Hsp90 machinery. Cold Spring Harb. Perspect. Biol. *11*, a034017.

Biebl, M.M., Riedl, M., and Buchner, J. (2020). Hsp90 co-chaperones form plastic genetic networks adapted to client maturation. Cell Rep *32*, 108063.

Biebl, M.M., Lopez, A., Rehn, A., Freiburger, L., Lawatscheck, J., Blank, B., Sattler, M., and Buchner, J. (2021). Structural elements in the flexible tail of the co-chaperone p23 coordinate client binding and progression of the Hsp90 chaperone cycle. Nat. Commun. 12, 828.

Blagosklonny, M.V., Toretsky, J., Bohen, S., and Neckers, L. (1996). Mutant conformation of p53 translated in vitro or in vivo requires functional HSP90. Proc. Natl. Acad. Sci. USA 93, 8379–8383.

Boczek, E.E., Reefschläger, L.G., Dehling, M., Struller, T.J., Häusler, E., Seidl, A., Kaila, V.R., and Buchner, J. (2015). Conformational processing of oncogenic v-Src kinase by the molecular chaperone Hsp90. Proc. Natl. Acad. Sci. USA 112, E3189–E3198.

Bose, S., Weikl, T., Bügl, H., and Buchner, J. (1996). Chaperone function of Hsp90-associated proteins. Science 274, 1715–1717.

Boysen, M., Kityk, R., and Mayer, M.P. (2019). Hsp70- and Hsp90-mediated regulation of the conformation of p53 DNA binding domain and p53 cancer variants. Mol. Cell 74, 831–843.e4.

Chen, S., and Smith, D.F. (1998). Hop as an adaptor in the heat shock protein 70 (Hsp70) and hsp90 chaperone machinery. J. Biol. Chem. 273, 35194–35200.

Chen, J.J., Nathaniel, D.L., Raghavan, P., Nelson, M., Tian, R., Tse, E., Hong, J.Y., See, S.K., Mok, S.A., Hein, M.Y., et al. (2019). Compromised function of the ESCRT pathway promotes endolysosomal escape of tau seeds and propagation of tau aggregation. J. Biol. Chem. 294, 18952–18966.

Cintron, N.S., and Toft, D. (2006). Defining the requirements for Hsp40 and Hsp70 in the Hsp90 chaperone pathway. J. Biol. Chem. 281, 26235–26244.

Dahiya, V., Agam, G., Lawatscheck, J., Rutz, D.A., Lamb, D.C., and Buchner, J. (2019). Coordinated conformational processing of the tumor suppressor protein p53 by the Hsp70 and Hsp90 chaperone machineries. Mol. Cell 74, 816–830.e7.

Delaglio, F., Grzesiek, S., Vuister, G.W., Zhu, G., Pfeifer, J., and Bax, A. (1995). NMRPipe: a multidimensional spectral processing system based on Unix pipes. J. Biomol. NMR 6, 277–293.

Dittmar, K.D., Hutchison, K.A., Owens-Grillo, J.K., and Pratt, W.B. (1996). Reconstitution of the steroid receptor.hsp90 heterocomplex assembly system of rabbit reticulocyte lysate. J. Biol. Chem. 271, 12833–12839.

Dittmar, K.D., Banach, M., Galigniana, M.D., and Pratt, W.B. (1998). The role of DnaJ-like proteins in glucocorticoid receptor.hsp90 heterocomplex assembly by the reconstituted hsp90.p60.hsp70 foldosome complex. J. Biol. Chem. 273, 7358–7366.

Dominguez, C., Boelens, R., and Bonvin, A.M. (2003). HADDOCK: a protein-protein docking approach based on biochemical or biophysical information. J. Am. Chem. Soc. 125, 1731–1737.

Echeverría, P.C., Bernthaler, A., Dupuis, P., Mayer, B., and Picard, D. (2011). An interaction network predicted from public data as a discovery tool: application to the Hsp90 molecular chaperone machine. PloS One 6, e26044.

Echtenkamp, F.J., Gvozdenov, Z., Adkins, N.L., Zhang, Y., Lynch-Day, M., Watanabe, S., Peterson, C.L., and Freeman, B.C. (2016). Hsp90 and p23 molecular chaperones control chromatin architecture by maintaining the functional pool of the RSC chromatin remodeler. Mol. Cell 64, 888–899.

Emsley, P., Lohkamp, B., Scott, W.G., and Cowtan, K. (2010). Features and development of Coot. Acta Crystallogr. D Biol. Crystallogr. 66, 486–501.

Evans, P.R., and Murshudov, G.N. (2013). How good are my data and what is the resolution? Acta Crystallogr. D Biol. Crystallogr. 69, 1204–1214.

Faust, O., Abayev-Avraham, M., Wentink, A.S., Maurer, M., Nillegoda, N.B., London, N., Bukau, B., and Rosenzweig, R. (2020). HSP40 proteins use class-specific regulation to drive HSP70 functional diversity. Nature 587, 489–494.

Finka, A., and Goloubinoff, P. (2013). Proteomic data from human cell cultures refine mechanisms of chaperone-mediated protein homeostasis. Cell Stress Chaperones 18, 591–605.

Freeman, B.C., and Morimoto, R.I. (1996). The human cytosolic molecular chaperones hsp90, hsp70 (hsc70) and hdj-1 have distinct roles in recognition of a non-native protein and protein refolding. EMBO J. 15, 2969–2979.

Freeman, B.C., Felts, S.J., Toft, D.O., and Yamamoto, K.R. (2000). The p23 molecular chaperones act at a late step in intracellular receptor action to differentially affect ligand efficacies. Genes Dev. 14, 422–434.

Fu, Q., Wang, W., Zhou, T., and Yang, Y. (2016). Emerging roles of NudC family: from molecular regulation to clinical implications. Sci. China Life Sci. 59, 455–462.

Genest, O., Hoskins, J.R., Kravats, A.N., Doyle, S.M., and Wickner, S. (2015). Hsp70 and Hsp90 of E. coli directly interact for collaboration in protein remodeling. J. Mol. Biol. 427, 3877–3889.

Gilbert, L.A., Larson, M.H., Morsut, L., Liu, Z., Brar, G.A., Torres, S.E., Stern-Ginossar, N., Brandman, O., Whitehead, E.H., Doudna, J.A., et al. (2013). CRISPR-mediated modular RNA-guided regulation of transcription in eukaryotes. Cell 154, 442–451.

Gilbert, L.A., Horlbeck, M.A., Adamson, B., Villalta, J.E., Chen, Y., Whitehead, E.H., Guimaraes, C., Panning, B., Ploegh, H.L., Bassik, M.C., et al. (2014). Genome-scale CRISPR-mediated control of gene repression and activation. Cell 159, 647–661.

Gocke, C.D., Osmani, S.A., and Miller, B.A. (2000). The human homologue of the Aspergillus nuclear migration gene nudC is preferentially expressed in dividing cells and ciliated epithelia. Histochem. Cell Biol. 114, 293–301.

Grammatikakis, N., Lin, J.H., Grammatikakis, A., Tsichlis, P.N., and Cochran, B.H. (1999). p50(cdc37) acting in concert with Hsp90 is required for Raf-1 function. Mol. Cell. Biol. 19, 1661–1672.

Hagn, F., Lagleder, S., Retzlaff, M., Rohrberg, J., Demmer, O., Richter, K., Buchner, J., and Kessler, H. (2011). Structural analysis of the interaction between Hsp90 and the tumor suppressor protein p53. Nat. Struct. Mol. Biol. 18, 1086–1093.

Hainzl, O., Lapina, M.C., Buchner, J., and Richter, K. (2009). The charged linker region is an important regulator of Hsp90 function. J. Biol. Chem. 284, 22559–22567.

Hernández, M.P., Chadli, A., and Toft, D.O. (2002). HSP40 binding is the first step in the HSP90 chaperoning pathway for the progesterone receptor. J. Biol. Chem. 277, 11873–11881.

Hessling, M., Richter, K., and Buchner, J. (2009). Dissection of the ATP-induced conformational cycle of the molecular chaperone Hsp90. Nat. Struct. Mol. Biol. 16, 287–293.

Horlbeck, M.A., Gilbert, L.A., Villalta, J.E., Adamson, B., Pak, R.A., Chen, Y., Fields, A.P., Park, C.Y., Corn, J.E., Kampmann, M., et al. (2016). Compact and highly active next-generation libraries for CRISPR-mediated gene repression and activation. eLife 5, e19760.

Jiang, Y., Rossi, P., and Kalodimos, C.G. (2019). Structural basis for client recognition and activity of Hsp40 chaperones. Science 365, 1313–1319.

Johnson, J.L. (2012). Evolution and function of diverse Hsp90 homologs and cochaperone proteins. Biochim. Biophys. Acta 1823, 607–613.

Johnson, B.D., Schumacher, R.J., Ross, E.D., and Toft, D.O. (1998). Hop modulates Hsp70/Hsp90 interactions in protein folding. J. Biol. Chem. 273, 3679–3686.

Johnson, J.L., and Toft, D.O. (1995). Binding of p23 and hsp90 during assembly with the progesterone receptor. Mol. Endocrinol. 9, 670–678.

Kabsch, W. (2010). Xds. Acta Crystallogr. D Biol. Crystallogr. 66, 125–132.

Kalinin, S., Valeri, A., Antonik, M., Felekyan, S., and Seidel, C.A. (2010). Detection of structural dynamics by FRET: a photon distribution and fluorescence lifetime analysis of systems with multiple states. J. Phys. Chem. B 114, 7983–7995.

Kampmann, M., Bassik, M.C., and Weissman, J.S. (2014). Functional genomics platform for pooled screening and generation of mammalian genetic interaction maps. Nat. Protoc. 9, 1825–1847.

Kirschke, E., Goswami, D., Southworth, D., Griffin, P.R., and Agard, D.A. (2014). Glucocorticoid receptor function regulated by coordinated action of the Hsp90 and Hsp70 chaperone cycles. Cell 157, 1685–1697.

Kravats, A.N., Hoskins, J.R., Reidy, M., Johnson, J.L., Doyle, S.M., Genest, O., Masison, D.C., and Wickner, S. (2018). Functional and physical interaction between yeast Hsp90 and Hsp70. Proc. Natl. Acad. Sci. USA *115*, E2210–E2219.

Kudryavtsev, V., Sikor, M., Kalinin, S., Mokranjac, D., Seidel, C.A., and Lamb, D.C. (2012). Combining MFD and PIE for accurate single-pair Forster resonance energy transfer measurements. ChemPhysChem *13*, 1060–1078.

Li, J., Richter, K., and Buchner, J. (2011). Mixed Hsp90-cochaperone complexes are important for the progression of the reaction cycle. Nat. Struct. Mol. Biol. *18*, 61–66.

Li, J., Richter, K., Reinstein, J., and Buchner, J. (2013). Integration of the accelerator Aha1 in the Hsp90 co-chaperone cycle. Nat. Struct. Mol. Biol. *20*, 326–331.

López, A., Elimelech, A.R., Klimm, K., and Sattler, M. (2021). The charged linker modulates the conformations and molecular interactions of Hsp90. Chembiochem *22*, 1084–1092.

Lorenz, O.R., Freiburger, L., Rutz, D.A., Krause, M., Zierer, B.K., Alvira, S., Cuéllar, J., Valpuesta, J.M., Madl, T., Sattler, M., et al. (2014). Modulation of the hsp90 chaperone cycle by a stringent client protein. Mol. Cell *53*, 941–953.

Mayer, M.P., and Bukau, B. (2005). Hsp70 chaperones: cellular functions and molecular mechanism. Cell. Mol. Life Sci. *62*, 670–684.

Mayer, M.P., and Le Breton, L. (2015). Hsp90: breaking the symmetry. Mol. Cell *58*, 8–20.

McCoy, A.J., Grosse-Kunstleve, R.W., Adams, P.D., Winn, M.D., Storoni, L.C., and Read, R.J. (2007). Phaser crystallographic software. J. Appl. Crystallogr. *40*, 658–674.

Morán Luengo, T., Kityk, R., Mayer, M.P., and Rüdiger, S.G.D. (2018). Hsp90 breaks the deadlock of the Hsp70 chaperone system. Mol. Cell *70*, 545–552.e9.

Müller, L., Schaupp, A., Walerych, D., Wegele, H., and Buchner, J. (2004). Hsp90 regulates the activity of wild type p53 under physiological and elevated temperatures. J. Biol. Chem. *279*, 48846–48854.

Nicholls, R.A., Long, F., and Murshudov, G.N. (2012). Low-resolution refinement tools in REFMAC5. Acta Crystallogr. D Biol. Crystallogr. *68*, 404–417.

Prodromou, C., Roe, S.M., O'Brien, R., Ladbury, J.E., Piper, P.W., and Pearl, L.H. (1997). Identification and structural characterization of the ATP/ADP-binding site in the Hsp90 molecular chaperone. Cell *90*, 65–75.

Prodromou, C., Siligardi, G., O'Brien, R., Woolfson, D.N., Regan, L., Panaretou, B., Ladbury, J.E., Piper, P.W., and Pearl, L.H. (1999). Regulation of Hsp90 ATPase activity by tetratricopeptide repeat (TPR)-domain co-chaperones. EMBO J. *18*, 754–762.

Prodromou, C., Panaretou, B., Chohan, S., Siligardi, G., O'Brien, R., Ladbury, J.E., Roe, S.M., Piper, P.W., and Pearl, L.H. (2000). The ATPase cycle of Hsp90 drives a molecular 'clamp' via transient dimerization of the N-terminal domains. EMBO J. *19*, 4383–4392.

Qi, L.S., Larson, M.H., Gilbert, L.A., Doudna, J.A., Weissman, J.S., Arkin, A.P., and Lim, W.A. (2013). Repurposing CRISPR as an RNA-guided platform for sequence-specific control of gene expression. Cell *152*, 1173–1183.

Richter, K., Muschler, P., Hainzl, O., Reinstein, J., and Buchner, J. (2003). Sti1 is a non-competitive inhibitor of the Hsp90 ATPase. Binding prevents the N-terminal dimerization reaction during the atpase cycle. J. Biol. Chem. *278*, 10328–10333.

Röhl, A., Wengler, D., Madl, T., Lagleder, S., Tippel, F., Herrmann, M., Hendrix, J., Richter, K., Hack, G., Schmid, A.B., et al. (2015). Hsp90 regulates the dynamics of its cochaperone Sti1 and the transfer of Hsp70 between modules. Nat. Commun. *6*, 6655.

Rosenzweig, R., Nillegoda, N.B., Mayer, M.P., and Bukau, B. (2019). The Hsp70 chaperone network. Nat. Rev. Mol. Cell Biol. *20*, 665–680.

Rüdiger, S., Germeroth, L., Schneider-Mergener, J., and Bukau, B. (1997). Substrate specificity of the DnaK chaperone determined by screening cellulose-bound peptide libraries. EMBO J. *16*, 1501–1507.

Rüdiger, S., Freund, S.M.V., Veprintsev, D.B., and Fersht, A.R. (2002). CRINEPT-TROSY NMR reveals p53 core domain bound in an unfolded form to the chaperone Hsp90. Proc. Natl. Acad. Sci. USA *99*, 11085–11090.

Rutz, D.A., Luo, Q., Freiburger, L., Madl, T., Kaila, V.R.I., Sattler, M., and Buchner, J. (2018). A switch point in the molecular chaperone Hsp90 responding to client interaction. Nat. Commun. *9*, 1472.

Sahasrabudhe, P., Rohrberg, J., Biebl, M.M., Rutz, D.A., and Buchner, J. (2017). The plasticity of the Hsp90 co-chaperone system. Mol. Cell *67*, 947–961.e5.

Sattler, M., Schleucher, J., and Griesinger, C. (1999). Heteronuclear multidimensional NMR experiments for the structure determination of proteins in solution employing pulsed field gradients. Progr. Nucl. Magn. Reson. Spectrosc. *34*, 93–158.

Schmid, A.B., Lagleder, S., Gräwert, M.A., Röhl, A., Hagn, F., Wandinger, S.K., Cox, M.B., Demmer, O., Richter, K., Groll, M., et al. (2012). The architecture of functional modules in the Hsp90 co-chaperone Sti1/Hop. EMBO J. *31*, 1506–1517.

Schrimpf, W., Barth, A., Hendrix, J., and Lamb, D.C. (2018). PAM: a framework for integrated analysis of imaging, single-molecule, and ensemble fluorescence data. Biophys. J. *114*, 1518–1528.

Schuck, P. (2000). Size-distribution analysis of macromolecules by sedimentation velocity ultracentrifugation and Lamm equation modeling. Biophys. J. *78*, 1606–1619.

Sepehrnia, B., Paz, I.B., Dasgupta, G., and Momand, J. (1996). Heat shock protein 84 forms a complex with mutant p53 protein predominantly within a cytoplasmic compartment of the cell. J. Biol. Chem. *271*, 15084–15090.

Shen, Y., and Bax, A. (2015). Protein structural information derived from NMR chemical shift with the neural network program TALOS-N. Methods Mol. Biol. *1260*, 17–32.

Simon, B., Madl, T., Mackereth, C.D., Nilges, M., and Sattler, M. (2010). An efficient protocol for NMR-spectroscopy-based structure determination of protein complexes in solution. Angew. Chem. Int. Ed. Engl. *49*, 1967–1970.

Smith, D.F., Sullivan, W.P., Marion, T.N., Zaitsu, K., Madden, B., McCormick, D.J., and Toft, D.O. (1993). Identification of a 60-kilodalton stress-related protein, p60, which interacts with hsp90 and hsp70. Mol. Cell. Biol. *13*, 869–876.

Suzuki, H., Noguchi, S., Arakawa, H., Tokida, T., Hashimoto, M., and Satow, Y. (2010). Peptide-binding sites as revealed by the crystal structures of the human Hsp40 Hdj1 C-terminal domain in complex with the octapeptide from human Hsp70. Biochemistry *49*, 8577–8584.

Taipale, M., Tucker, G., Peng, J., Krykbaeva, I., Lin, Z.Y., Larsen, B., Choi, H., Berger, B., Gingras, A.C., and Lindquist, S. (2014). A quantitative chaperone interaction network reveals the architecture of cellular protein homeostasis pathways. Cell *158*, 434–448.

Tian, R., Gachechiladze, M.A., Ludwig, C.H., Laurie, M.T., Hong, J.Y., Nathaniel, D., Prabhu, A.V., Fernandopulle, M.S., Patel, R., Abshari, M., et al. (2019). CRISPR interference-based platform for multimodal genetic screens in human iPSC-derived neurons. Neuron *104*, 239–255.e12.

Tugarinov, V., Hwang, P.M., Ollerenshaw, J.E., and Kay, L.E. (2003). Cross-correlated relaxation enhanced 1H–13C NMR spectroscopy of methyl groups in very high molecular weight proteins and protein complexes. J. Am. Chem. Soc. *125*, 10420–10428.

Verba, K.A., Wang, R.Y., Arakawa, A., Liu, Y., Shirouzu, M., Yokoyama, S., and Agard, D.A. (2016). Atomic structure of Hsp90-Cdc37-Cdk4 reveals that Hsp90 traps and stabilizes an unfolded kinase. Science *352*, 1542–1547.

Vranken, W.F., Boucher, W., Stevens, T.J., Fogh, R.H., Pajon, A., Llinas, M., Ulrich, E.L., Markley, J.L., Ionides, J., and Laue, E.D. (2005). The CCPN data model for NMR spectroscopy: development of a software pipeline. Proteins *59*, 687–696.

Wandinger, S.K., Suhre, M.H., Wegele, H., and Buchner, J. (2006). The phosphatase Ppt1 is a dedicated regulator of the molecular chaperone Hsp90. EMBO J. *25*, 367–376.

Wang, R.Y.-R., Noddings, C.M., Kirschke, E., Myasnikov, A.G., Johnson, J.L., and Agard, D.A. (2020). GR chaperone cycle mechanism revealed by cryo-EM:

inactivation of GR by GR:Hsp90:Hsp70:Hop client-loading complex. bioRxiv. https://doi.org/10.1101/2020.11.05.370247.

Wegele, H., Wandinger, S.K., Schmid, A.B., Reinstein, J., and Buchner, J. (2006). Substrate transfer from the chaperone Hsp70 to Hsp90. J. Mol. Biol. 356, 802–811.

Wentink, A.S., Nillegoda, N.B., Feufel, J., Ubartaitė, G., Schneider, C.P., De Los Rios, P., Hennig, J., Barducci, A., and Bukau, B. (2020). Molecular dissection of amyloid disaggregation by human HSP70. Nature 587, 483–488.

Winn, M.D., Ballard, C.C., Cowtan, K.D., Dodson, E.J., Emsley, P., Evans, P.R., Keegan, R.M., Krissinel, E.B., Leslie, A.G., McCoy, A., et al. (2011). Overview of the CCP4 suite and current developments. Acta Crystallogr. D Biol. Crystallogr. 67, 235–242.

Xu, Y., Singer, M.A., and Lindquist, S. (1999). Maturation of the tyrosine kinase c-src as a kinase and as a substrate depends on the molecular chaperone Hsp90. Proc. Natl. Acad. Sci. USA 96, 109–114.

Xu, W., Beebe, K., Chavez, J.D., Boysen, M., Lu, Y., Zuehlke, A.D., Keramisanou, D., Trepel, J.B., Prodromou, C., Mayer, M.P., et al. (2019). Hsp90 middle domain phosphorylation initiates a complex conformational program to recruit the ATPase-stimulating cochaperone Aha1. Nat. Commun. 10, 2574.

Yang, Y., Yan, X., Cai, Y., Lu, Y., Si, J., and Zhou, T. (2010). NudC-like protein 2 regulates the LIS1/dynein pathway by stabilizing LIS1 with Hsp90. Proc. Natl. Acad. Sci. USA 107, 3499–3504.

Zhang, M., Botër, M., Li, K., Kadota, Y., Panaretou, B., Prodromou, C., Shirasu, K., and Pearl, L.H. (2008). Structural and functional coupling of Hsp90- and Sgt1-centred multi-protein complexes. EMBO J. 27, 2789–2798.

Zheng, M., Cierpicki, T., Burdette, A.J., Utepbergenov, D., Janczyk, P.Ł., Derewenda, U., Stukenberg, P.T., Caldwell, K.A., and Derewenda, Z.S. (2011). Structural features and chaperone activity of the NudC protein family. J. Mol. Biol. 409, 722–741.

Zhu, X.J., Liu, X., Jin, Q., Cai, Y., Yang, Y., and Zhou, T. (2010). The L279P mutation of nuclear distribution gene C (NudC) influences its chaperone activity and lissencephaly protein 1 (LIS1) stability. J. Biol. Chem. 285, 29903–29910.

STAR★METHODS

KEY RESOURCES TABLE

REAGENT or RESOURCE	SOURCE	IDENTIFIER
Antibodies		
Anti-stip1	Sigma-Aldrich	Cat# AV46164; RRID:AB_1857582
Anti-betaActin	CST	Cat# 8H10D10; RRID:AB_2242334
IRDye® 680RD Goat anti-Rabbit IgG Secondary Antibody	Licor	Cat# 926-68071; RRID:AB_10956166
IRDye® 800CW Goat anti-Mouse IgG Secondary Antibody	Licor	Cat# 926-32210; RRID:AB_621842
Bacterial and virus strains		
BL21 (DE3)	Sigma-Aldrich	Cat#: CMC0014
BL21-CodonPlus (DE3)-RIL	Agilent	Cat#: 230245
Rosetta 2 (DE3)	Sigma-Aldrich	Cat#: 71400
Chemicals, peptides, and recombinant proteins		
Dexamethasone	Sigma-Aldrich	Cat#: D4902
ATP	Sigma-Aldrich	Cat# A26209
AMP-PNP	Sigma-Aldrich	Cat# 10102547001
ADP	Sigma-Aldrich	Cat# 01905
3-(2-Iodacetamido)-PROXYL	Sigma-Aldrich	Cat# 253421
Atto-532 maleimide	ATTO-TEC	Cat#: AD 532-45
Alexa Fluor 647 C2 Maleimide	Thermo Fisher Scientific	Cat#: A20347
Dexamethasone Fluorescein	Thermo Fisher Scientific	Cat#: D1383
Alexa Fluor 488	Thermo Fisher Scientific	Cat#: A10254
2-Ketobutyric Acid-4-13C, 3,3-d2	Cortecnet	Cat# : CCD1410P025
L-Methionine 2,3,3,4,4-D5, Methyl-13CH3	Cambridge Isotope	Cat# : CDLM-8885
Alpha-Ketoisovaleric Acid, Sodium Salt (3-Methyl-13C; 3,4,4,4-D4)	Cambridge Isotope	Cat# : CDLM-7317
Critical commercial assays		
SensiFAST™ cDNA Synthesis Kit	Meridian Biosciences, Bioline	Cat#: Bio-65054
SensiFAST SYBR Lo-ROX reagents	Meridian Biosciences, Bioline	Cat#: Bio-94005
Deposited data		
Structure DNAJB1^{CTDs} / NudC$^{100-141}$	PDB	7NDX
Experimental models: Cell lines		
K562-SFFV-dCas9-NLS$_{2x}$-BFP-KRAB-GR-2xGRE-mADH	This work	N/A
Oligonucleotides		
NudC#1: GGCGGACGACTAGAGTCGTT; NudC#2: GGCAGGAGCGTAGAGAGCGC;	Eurofins	N/A
Hop#1: GCGGTGGCCAGGCCGCGGTA; Hop#2: GCCCTGAAGGCGTCCCGAGG;	Eurofins	N/A
non-targeting#1: GTCCACCCTTATCTA GGCTA; non-targeting#2: GGACTAAGC GCAAGCACCTA	Eurofins	N/A
NudC-F: GTGACTGTGCATCTGGAGAAG, NudC-R: CTTGGTGTTGATCTCAGGGTC,	Eurofins	N/A

(Continued on next page)

Continued

REAGENT or RESOURCE	SOURCE	IDENTIFIER
Hop-F: TGGAACAGATGCAGAAGGAC, Hop-R: CATGAGGGCGAAGGGAAG,	Eurofins	N/A
Actin-F: ACCTTCTACAATGAGCTGCG, Actin-R: CCTGGATAGCAACGTACATGG.	Eurofins	N/A
Recombinant DNA		
pET28a-hHsp90b	Tippel F., TU Munich	N/A
pET28-Hop	Richter K., TU Munchen	N/A
pET23-p23	D. Toft	N/A
pETSumo-hHsp70	Kriehuber E., TU Munchen	N/A
pETSumo-ydj1	Schmid A., TU Munchen	N/A
pETSumo-NudC	This study	N/A
pET28-NudC	This study	N/A
pET28-NudC 1-141	This study	N/A
pET28-NudC 100-141	This study	N/A
pET28-NudC 158-274	This study	N/A
pET28-NudC 158-331	This study	N/A
pET28-NudC 50-331	This study	N/A
pET28-NudC 1-274	This study	N/A
pET28 NudC I104A/L107A	This study	N/A
pET28 hHSP90 Md	This study	N/A
pET28 hHSP90 NM	This study	N/A
pET28 hHSP90 MC	This study	N/A
pET28 hHSP90 322-328GS	This study	N/A
pET28-p53-DBD	Dahiya V., TU Munchen	N/A
pET28-p53-DBD-C182-C229	Dahiya V., TU Munchen	N/A
pETSumo-DNAJB1	Rosenzweig R., Weizmann Institute	N/A
pET29b- DNAJB1CTDs	Rosenzweig R., Weizmann Institute	N/A
pETSumo-Ydj1 Mono	Rosenzweig R., Weizmann Institute	N/A
pETHalo-GR-LBDm	Rutz D., TU Munich	N/A
pETSumo-hHSP90a	Tippel F., TU Munich	N/A
Software and algorithms		
HADDOCK/CNS	(Dominguez et al., 2003)	https://www.bonvinlab.org/software/haddock2.2/
TALOS-N	(Shen and Bax, 2015)	https://spin.niddk.nih.gov/bax/software/TALOS-N/
NMRpipe	(Delaglio et al., 1995)	https://www.ibbr.umd.edu/nmrpipe/index.html
ccpNmr Analysis 2.5.2	(Vranken et al., 2005)	https://ccpn.info/software/version-2/version-2-downloads/
RANCH	(Bernadó et al., 2007)	https://www.embl-hamburg.de/biosaxs/download.html
CCP4	(Winn et al., 2011)	https://www.ccp4.ac.uk/download/
REFMAC	(Nicholls et al., 2012)	N/A
Coot	(Emsley et al., 2010)	N/A
Phaser	(McCoy et al., 2007)	N/A
Sedview / SedFit	(Schuck, 2000)	http://www.rasmb.org/
OriginPro	OriginLab	https://www.originlab.com/
PAM	(Schrimpf et al., 2018)	https://gitlab. com/PAM-PIE/PAM
MAGeCK-iNC (MAGeCK-including Negative Controls)	(Tian et al., 2019)	N/A

RESOURCE AVAILABILITY

Lead contact
Further information and requests for resources and reagents should be directed to and will be fulfilled by the lead contact, Prof. Johannes Buchner (johannes.buchner@tum.de).

Material availability
Plasmids generated in this study will be made available on request, but we may require a payment and/or a completed Materials Transfer Agreement if there is potential for commercial application.

Data and code availability
- All data are available from the corresponding authors and/or included in the manuscript. The atomic coordinates for the NudC/DNAJB1 complex have been deposited to the Protein Data Bank with the accession number PDB: 7NDX.
- The custom software package PAM was used for the analysis of the single-pair FRET experiments (Schrimpf et al., 2018). The code is freely distributed as open-source software under https://www.cup.uni-muenchen.de/pc/lamb/software/pam.html and hosted at https://gitlab.com/PAM-PIE/PAM.
- Any additional information required to reanalyze the data reported in this paper is available from the lead contact upon request.

EXPERIMENTAL MODEL AND SUBJECT DETAILS

Cell lines and plasmids
K562 cell lines were cultured in in RPMI-1640 with 25 mM HEPES and 2.0 g/l $NaHCO_3$ in 10% FBS, 2 mM glutamine, 100 units/ml penicillin and 100 µg/ml streptomycin. The K562 cell line contained a lentivirally transduced SFFV-dCas9-NLS_{2x}-BFP-KRAB expression cassette as published previously (Gilbert et al., 2013). The GR sequence was inserted into the pMK1253 (Chen et al., 2019) plasmid digested with NheI and BsrGI using Sequence and Ligation Independent Cloning (SLIC). A GR reporter construct was amplified from pDLO-2xGal4-2xGRE-mADH containing reporter plasmid (kind gift from Brian Freeman) using SLIC with the P1: gatcgataagcttgatatcgaattcGTTTTCCCAGTCACGACG P2: ctcgcccttgctcaccatggcgcgccTTTACCAACAGTACCGGAATG primer pair. All *in vivo* experiments were conducted with the K562 cell line carrying the GR expression cassette and the reporter construct as well as the dCas9 construct unless specified otherwise. Individual sgRNAs were cloned into the pLG15 or pSLQ1371 plasmid backbone digested with BlpI and BstXI using annealed oligos (NudC#1: GGCGGACGACTAGAGTCGTT; NudC#2: GGCAGGAGCGTAGAGAGCGC; Hop#1: GCGGTGGCCAGGCCGCGGTA; Hop#2: GCCCTGAAGGCGTCCCGAGG; non-targeting#1: GTCCACCCTTATCTAGGCTA; non-targeting#2: GGACTAAGCGCAAGCACCTA). For protein expression, *E. coli* BL21 DE3 cells were used. The $NudC^{WT}$ gene and the $NudC^{50-331}$ mutant were synthesized and cloned into the pET28b vector using the GeneArt service (ThermoFisher). The other truncations of NudC were cloned into pET28b between the BamHI and XhoI cloning sites using SLIC.

METHOD DETAILS

CRISPRi library design
A pooled CRISPRi sgRNA library targeting 357 genes involved in proteostasis with 5 sgRNAs per gene and 250 non-targeting sgRNAs was designed as previously described (Horlbeck et al., 2016). Oligonucleotide pools were synthesized by Agilent, amplified by PCR and cloned into sgRNA expression plasmids as previously described (Table S3) (Gilbert et al., 2014).

CRISPRi screening for modulators
For pooled screening of the sgRNA library, 7.5 million Hek293T cells were seeded into 15-cm^2 dishes in complete DMEM on day 0. On day 1, 5 µg of library plasmid was transfected along with 5 µg of packaging mix (Kampmann et al., 2014) using calcium phosphate co-precipitation transfection. The medium was exchanged after about 8 h and cells were incubated at 37 °C. To harvest the virus, the supernatant was filtered through a syringe-driven 0.45 µm filter on day 3. The virus was concentrated by ultrafiltration with a 100 kDa cutoff. The virus was then resuspended in 12 mL of RPMI-1640 medium and the resulting virus-suspension was used to resuspend $20x10^6$ K562 cells. Cells were supplemented with 8 µg/mL polybrene and seeded into T175 flasks with $10x10^6$ cells per flask. After 48 h, the infection rate was determined and positives were selected by addition of 0.8 mg/mL puromycin. Puromycin treatment was stopped 72 h before sorting. Cells were recovered for 48 h and then treated with 1 nM dexamethasone over-night. Cells were then sorted using an Aria II FACS cytometer into high-mCherry and low-mCherry populations. Genomic DNA was isolated using a NucleoSpin Blood Kit according to the manufacturer's protocol. Then, the sgRNA-encoding region was PCR-amplified and sequenced using next-generation sequencing as previously described (Gilbert et al., 2014). Phenotypes and p values were extracted using a previously published bioinformatics pipeline (Table S3) (Tian et al., 2019).

In vivo GR activity measurement

To test GR activity, we cloned sgRNAs targeting Hop and NudC as well as non-targeting sgRNAs into pLG15 or pSLQ1371 vectors (Gilbert et al., 2014). K562 cells were then transduced with the sgRNA-expressing plasmid by lentiviral infection. 10 days after transduction, we treated cells with 10 nM dexamethasone for 24 h. Mean mCherry fluorescence was measured by flow cytometry (BD FACSCelesta) and normalized to the non-targeting control. Experiments were conducted in biological triplicates.

In vivo viability analysis of knockdown strains

To measure viability after knockdown of NudC or Hop, the K562 cells were lentivirally transduced with the sgRNA-expressing plasmid, containing a BFP-expression cassette for selection. The fraction of BFP$^+$ cells was quantified by flow cytometry (BD FACS-Celesta) on different days after infection. Experiments were conducted in biological triplicates.

RT-qPCR

Total RNA was extracted using the Quick-RNA Miniprep Kit (Zymo Research, R1054), and first-strand cDNA was synthesized with the SensiFAST^{TM} cDNA Synthesis Kit (Bioline, Bio-65054). RT-qPCR was performed with SensiFAST SYBR Lo-ROX reagents (Bioline, #BIO-94005). Fold changes in expression were calculated using the $\Delta\Delta C_t$ method. RT-qPCR primers used were: NudC-F: GTGACTGTG-CATCTGGAGAAG, NudC-R: CTTGGTGTTGATCTCAGGGTC, Hop-F:TGGAACAGATGCAGAAGGAC, Hop-R: CATGAGGGCGAAGG-GAAG, Actin-F: ACCTTCTACAATGAGCTGCG, Actin-R: CCTGGATAGCAACGTACATGG.

Western Blot

Cells were lysed using RIPA buffer (Thermo Fisher Scientific, #89900). Total protein was quantified using a Pierce BCA Protein Assay Kit (Thermo Fisher Scientific, #23225). Samples were subjected to SDS–PAGE on NuPage 4–12% Bis-tris gels (Thermo Fisher Scientific, #NP0336BOX) and transferred to a nitrocellulose membrane (Bio-Rad, #1704271). The primary antibodies used in this study were: rabbit anti-STIP1(Sigma, #11815, 1:1000), mouse anti-β-actin (Cell Signaling Technologies, #3700, 1:2,000). Blots were incubated with LI-COR secondary antibodies and imaged using an Odyssey Fc Imaging system (LI-COR, #2800). Digital images were processed and analysed using LI-COR ImageStudio software.

Protein expression and purification

NudC and mutants were expressed in *E. coli* BL21 DE3 cells by induction with 1 mM IPTG and expression for 4 h at 37 °C before harvesting. Cells were then resuspended in Ni-NTA Buffer (10 mM Tris, pH 7.5, 50 mM KCl, 50 mM NaCl, 5 mM MgCl$_2$, 1 mM DTT, 10 mM imidazole), lysed by pressure and subjected to affinity chromatography on a Ni-NTA column. The bound proteins were washed with 2 mM ATP dissolved in Ni-NTA buffer before elution with Ni-NTA buffer supplemented with 300 mM imidazole. Subsequently, proteins were subjected to size exclusion chromatography in 40 mM Hepes, 150 mM KCl, 5 mM MgCl$_2$, 1 mM DTT, pH 7.5. All experiments with GR-LBD were conducted with the stabilized, purified GR-LBDm as previously published (Dahiya et al., 2019). Hsp70, Hop, p23, GR-LBDm, Ydj1 and mutants, Hsp90α and Hsp90β were purified as described previously (Dahiya et al., 2019; Lorenz et al., 2014). Hop mutants were a kind gift from Daniel A. Rutz.

NMR

All NMR experiments were performed on Bruker Avance III spectrometers equipped with cryogenically cooled TCI probeheads, operating at magnetic field strengths corresponding to ^{1}H Larmor frequencies of 950, 900, 800 or 600 MHz. Sample temperature was set at 303 K for all experiments. ^{1}H,^{15}N correlation experiments were performed in 40 mM phosphate buffer, 100 mM NaCl, 2 mM DTT, pH 6.8, 8% D$_2$O, while methyl-labeled experiments were all performed in Hepes 40 mM, KCl 100 mM, MgCl$_2$ 2 mM, TCEP 0.5 mM, pH 7.5 in 100% D$_2$O. All data were processed with NMR pipe (Delaglio et al., 1995) and analyzed in CCPNMR (Vranken et al., 2005).

Chemical shift assignments

The backbone assignment of all NudC and Hsp90 constructs was performed using standard 3D heteronuclear experiments HNCACB, HNCA, CBCA(CO)NH or (H)C(CCO)NH, HNCO and HN(CA)CO (Sattler et al., 1999). Secondary structure predictions based on ^{13}Cα, ^{13}Cβ, ^{13}C' secondary chemical shifts were performed using TalosN (Shen and Bax, 2015). The assignment of NudC methyl resonances was performed on ^{1}H, ^{13}C, ^{15}N uniformly labeled samples using ^{1}H-^{13}C HMQC methyl-TROSY (Tugarinov et al., 2003), (H)C(CCO)NH and H(CCCO)NH correlation experiments. To assign the Hsp90 methyl resonances of the isolated domains (NTD, MD and CTD) their backbone resonances were first assigned. Methyl assignments were subsequently transferred by matching ^{13}Cα, ^{13}Cβ frequencies from backbone experiments, and CCH-TOCSY experiments in methyl-labeled, ^{13}C, ^{2}H uniformly labeled samples. The individual domain assignment was further validated based on the structure of the domains and their HMQC-NOESY-HMQC 3D spectrum with a 200 ms evolution delay. Methyl groups in full-length Hsp90 were assigned by transferring the assignment from the isolated domain and validated using a 3D HMQC-NOESY-HMQC spectrum with a 200 ms NOE mixing time.

Titrations

Titrations were performed with proteins purified in identical buffers. The assignment of fully bound-forms, used to determine chemical shifts perturbations, was performed from the successive addition of binding partners and following the chemical shift perturbations. The titration on the isolated Hsp90-MD was done on a ^{15}N-labeled, 66% partially deuterated proteins concentrated at 180 μM with addition of NudC$^{158-274}$ or NudC$^{158-331}$ in 7 steps up to a saturation of 1:5 and 1:4 respectively. Titration on NudC$^{158-274}$ and

NudC[158-331] were performed with ^{15}N-labeled samples concentrated to 150 µM with a 5 steps addition of Hsp90-MD up to 1:4 excess. Determination of DNAJB1 binding site to NudC was performed using ^{15}N-labeled NudC[1-141] with a single addition of DNAJB1[CTDs] at 205 µM. The experiment was also performed with NudC[60-141] with three successive additions of DNAJB1[CTDs] at 29 µM, 59 µM and 295 µM. Determination of GR binding site to NudC was performed using ^{15}N-labeled NudC[158-331] at 220 µM and with addition of 70 µM and 35 µM of GR-LBD and using ^{15}N-labeled NudC[158-331] at 105 µM with addition of premixed GR-LBD/DNAJB1[CTDs] with respective concentrations of 50 µM / 200 µM for the first point and 25 µM / 100 µM for the second. Perturbations and intensity changes on Hsp90 [13]CH$_3$-labeled were measured at 95 µM with single addition of NudC at 1:1 excess, of NudC[1-274] at 1:2, of NudC[154-331] at 1:2 and of NudC[1-141] at 1:1.25. Intensity changes on NudC [13]CH$_3$-labeled were measured either at 37 µM with addition of Hsp90 with a 1:1 excess and addition of DNAJB1 to a 1:1:2 excess or with NudC at 50 µM with addition of DNAJB1 and GR-LBD with a molar ratio of 1:0.34, DNAJB1[CTDs] at 1:1 and DNAJB1[CTDs]/GR-LBD at 1:1:0.34. In the plot, intensities were corrected for NudC dilution. All chemical shift perturbations were calculated as a weighted average following the equations $CSP = ((\Delta^1H)^2 + (\Delta^{15}N*0.159)^2)^{1/2}$ for ^{1}H, ^{15}N spectra and $CSP = ((\Delta^1H)^2 + (\Delta^{13}C*0.3)^2)^{1/2}$ for ^{1}H, ^{13}C spectra.

Paramagnetic relaxation enhancements (PRE)
NudC[154-274] was first exchanged to NMR-buffer without DTT using a PD10 buffer exchange column (GE Healthcare, Buckinghamshire, UK). IPSL (N-(1-oxyl-2,2,5,5-tetramethyl-3-pyrrolidinyl)iodoacetamide) was added to a 10 times molar excess to the NudC[154-274] in non-reduced buffer and incubated overnight at room temperature and protected from light. The excess spin label was removed using a PD10 column. 200 µM of NudC[154-274] IPSL-labeled was added to ^{15}N, ^{2}H labeled Hsp90[MD] at 100 µM. Data were recorded using ^{1}H,^{15}N TROSY-HSQC experiment with a recycling delay of 4s. 10 times molar excess of fresh ascorbic acid was added to reduce the paramagnetic probe and the experiment was repeated using the same parameters to record the reference experiment in the absence of PRE (Battiste and Wagner, 2000).

Calculation of structural models
HADDOCK
The structural model of the Hsp90[MD]/NudC[CS] complex was calculated using HADDOCK/CNS (Dominguez et al., 2003). The crystal structures of the isolated Hsp90[MD] (PDB: 3PRY) and of the isolated NudC[CS] (PDB: 3QOR) were used as starting points. Chemical shift perturbations (CSPs) were used to define ambiguous restraints: residues with CSP>0.043 for Hsp90[MD] and CSP>0.072 for NudC[155-274] and for which the solvent accessibility is >50%, as defined by NACCESS, were used as active restraints; residues neighboring the active ones or with significant CSP but not validating solvent accessibility were defined as passives. Default values for the number of generated structures were increased to 2000 for the rigid-body docking stage (default 1000) and to 500 for the flexible and solvent refinement stage (default 200). Structures generated by HADDOCK after solvent refinement were clustered according to an FCC cut-off of 0.75 and a minimum number of members in a cluster of 4. The full-length Hsp90/NudC[CS] model was obtained by aligning the Hsp90[MD] from the HADDOCK model to a structure of the full-length Hsp90 dimer in a closed conformation (PDB: 5FWK).

Back calculation of PREs intensity ratio
Theoretical PRE effects on Hsp90[MD] induced by NudC[CS] binding were calculated based on the structures obtained from HADDOCK docking. The four best scoring structures of the ensemble were used. For each structure, four different conformations of IPSL covalently bound to C188 were generated in ARIA following protocol from Simon et al. (Simon et al., 2010). For each structure and conformation, the distance between the paramagnetic center and the backbone NH of Hsp90[MD] were extracted. The relaxation ratio was calculated as described (Battiste and Wagner, 2000; Simon et al., 2010) for each conformation, assuming a tumbling correlation τ_c of 30 ns, an [1]H-R_2 transverse relaxation rate of 35 s^{-1} and a complex population of 70%. The 16 conformations were then averaged to obtain the final values.

RANCH random linker modeling
The 2:2:2 ternary complex between HSP90, DNAJB1[CTD] and NudC was generated based on the Hsp90/NudC[CS] model and the DNAJB1[CTD]/NudC[100-141] structure. The relative positions of the two bound molecules of NudC[CS] and NudC[100-141] from each complex was kept fixed while the position of each complex was kept free. The linker connecting the end of NudC[100-141] to the start of NudC[CS] was generated as dummy residues following a random-coil model using RANCH (Bernadó et al., 2007).

Crystallography
Initial screening of crystallization conditions was carried out by the vapor diffusion method. Sitting drops were set up using 400 nL of a 1:1 mixture of protein and crystallization solutions. The co-crystallization was performed using DNAJB1[CTDs] concentrated to 20 mg/ml and an excess of NudC[100-141]. Crystals were obtained at 20°C from a solution containing 0.1 M of sodium acetate trihydrate pH 4.0 and 15% (v/v) of polyethylene glycol 400. Single crystals were cryoprotected using 25% ethylene glycol in the mother solution and flash-frozen in liquid nitrogen. The diffraction data were collected at the X06DA beamline at the Swiss Light Source (Paul Scherrer Institut, Villigen, Switzerland). The data were indexed and integrated using the XDS program package (Kabsch, 2010) and scaled and merged using the Aimless program (Evans and Murshudov, 2013). The initial phases were obtained by molecular replacement, calculated using Phaser software (McCoy et al., 2007) and the DNAJB1[CTD] structure extracted from the DNAJB1[CTDs]:HSP70 complex (PDB: 3AGY, chain A) (Suzuki et al., 2010). All crystallographic calculations were carried within the CCP4 program suite (Winn et al., 2011). The protein structure was refined with the program REFMAC (Nicholls et al., 2012) and manual adjustments were made to the models using Coot (Emsley et al., 2010). The crystallographic parameters, data statistics and refinement parameters are shown in the Table S2.

Atomic coordinates and structure factors for the DNAJB1[CTDs]/NudC[100-141] complex have been deposited in the RCSB Protein Data Bank with pdb code PDB: 7NDX.

Analytical Ultracentrifugation

Sedimentation velocity experiments were performed in a ProteomLab Beckman XL-A centrifuge (Beckman Coulter, Brea, California) equipped with an AVIV fluorescence detection unit (Aviv Inc., Lakewood, USA). Experiments were performed at 20 °C and 42,000 rpm in an An-50 Ti rotor (Beckman Coulter, Brea, California). Usually 300 scans were recorded, in a total measurement time of approximately 6 h. For the experiments, 500 nM of Atto488-maleimide (ATTO-TEC) labeled protein was detected in aUC buffer (20 mM Hepes, 20 mM KCl, 5 mM MgCl$_2$, 5 mM DTT, pH 7.5). Protein concentrations were used as indicated in the figure legends. In experiments with pre-formed complexes, the components were incubated for 60 min at room temperature for complex formation. For most experiments we used Hsp90α and Ydj1 as the Hsp40 isoform, unless specified otherwise. Nucleotides were used at a concentration of 2 mM when applicable and measurements that contained the GR-LBD were supplemented with 50 μM dexamethasone. Data analysis was performed using Sedview, SedFit (Schuck, 2000) and Origin Pro 2016G.

Single-pair FRET experiments

Single-pair FRET experiments were conducted as described previously (Dahiya et al., 2019). Briefly, 10 nM of p53-DBD labeled with Atto532 and Alexa647 was incubated with 3 μM Hsp40 (Ydj1), 20 μM Hsp70 and 5 mM ATP at 37 °C for 1 h in 20 mM Hepes, 50 mM KCl, 5 mM MgCl$_2$ and 1 mM TCEP at pH 7.4. Subsequently, the labeled p53-DBD concentration was diluted in the same buffer to approximately 70 pM for the spFRET measurements while keeping the Hsp40, Hsp70 and ATP concentrations the same as that used for the initial incubation. NudC, Hsp90α or Hop was added to a final concentration of 20 μM each after pre-incubation with Hsp40/Hsp70/ATP at 37°C. Measurements were performed at room temperature on a custom build confocal microscope as described in (Dahiya et al., 2019). The apparatus combines multi-parameter fluorescence detection (MFD) with pulsed interleaved excitation (PIE), which enables the calculation of stoichiometry, FRET efficiency, fluorescence lifetime and anisotropy for each burst simultaneously. With MFD-PIE, it is also possible to determine the appropriate correction factors for accurate spFRET experiments from the same data (Kudryavtsev et al., 2012). Sub-millisecond conformational dynamics in the spFRET experiments were visualized by plotting the intensity based FRET efficiency versus donor fluorescence lifetime (Kalinin et al., 2010). Briefly, the FRET efficiency (E) can be determined from the donor and acceptor fluorescence intensities:

$$E = \frac{I_A}{\gamma I_D + I_A}$$

where I_A is the fluorescence intensity of the acceptor corrected for background, direct excitation and spectral crosstalk, I_D is the background corrected donor signal and γ is the detection correction factor to adjust for different sensitivities between the two fluorophores.

FRET efficiency is also related to the fluorescence lifetime of donor as $E = 1 - (\tau_{D(A)}/\tau_{D(0)})$ where $\tau_{D(A)}$ and $\tau_{D(0)}$ are the fluorescence lifetime of donor in the presence and absence of an acceptor respectively. These relationships are true when the molecular conformations are static over the burst duration. When molecular conformations fluctuate between the two different states with different FRET efficiencies, the intensity-based FRET efficiency is a species weighted value dependent on the two FRET efficiencies and the time spent in the respect states. For the measured donor fluorescence lifetime, a photon-weighted average is measured (i.e. dependent on the lifetime and number of detected photons). For donor florescence lifetimes of τ_1 and τ_2 for the two FRET states, the determined FRET efficiency is given by $E = (\tau_1.\tau_2/\tau_{D(0)}[\tau_1 + \tau_2 - \tau])$ where τ is the fluorescence weighted average donor lifetime. As more donor photons are emitted from the lower FRET efficiency state, this leads to a shift of the lifetime-determined FRET efficiency to the right of the static FRET line.

p53-DBD Aggregation Assay

Aggregation kinetics were monitored in a Cary 100 UV-visible spectrophotometer (Varian). 1.5 μM of p53-DBD were incubated with 2 μM Hsp40, 10 μM Hsp70 and 5 mM ATP at 37°C for 1 h in 20 mM Hepes pH 7.4, 50 mM KCl, 5 mM MgCl$_2$ and 1mM TCEP buffer. Light scattering at 350 nm was continuously monitored at 37 °C after addition of 10 μM NudC and/or 12 μM Hsp90β.

Fluorescence Anisotropy

Hormone binding to the GR-LBD was monitored as described previously (Kirschke et al., 2014). Briefly, for equilibrium GR-LBD measurements, 1 μM of apo GR-LBD was mixed with 2 μM Hsp40 (Ydj1), 12 μM Hsp70, 5 mM ATP and 12 μM of the indicated (co)-chaperones in 30 mM Hepes pH 7.5, 50 mM KCl, 5 mM MgCl$_2$, 2 mM DTT buffer and incubated at room temperature for 60-70 min. Experiments were performed with Hsp90α. F-Dex was added in a final concentration of 100 nM and the binding of F-Dex to the GR-LBD was monitored at 25 °C by measuring the fluorescence anisotropy values. For the analysis, the start-value immediately after addition of F-Dex was subtracted from the trace to show the Δ-anisotropy values. Data were fit with a single-exponential fit using OriginPro 2016G.

For timed-addition experiments, 1 μM apo GR-LBD was mixed with 100 nM F-Dex in 30 mM Hepes pH 7.5, 50 mM KCl, 5 mM MgCl$_2$, 2 mM DTT and the binding of F-Dex to GR-LBD was monitored by measuring the fluorescence anisotropy at 25 °C. After about

50 min, Hsp40 (Ydj1), Hsp70 and ATP were added to a final concentration of 1.83 μM, 11.1 μM and 4.6 mM, respectively, and fluorescence anisotropy was monitored. After allowing dissociation of hormone for 50 – 60 min, NudC, Hsp90α, Hop or p23 were added as indicated in the figures. The concentrations used for timed-addition experiments with NudC and Hsp90 were at 16.5 μM and 13.6 μM, respectively. In timed-addition experiments with Hop, p23 and Hsp90, the concentrations used were 10 μM, 12 μM and 12 μM, respectively.

Fluorescence Polarization

Steady-state equilibrium binding of Hsp40 to NudC was measured by fluorescence polarization using 100 nM of Hsp40 (Ydj1), fluorescently tagged with Alexa Fluor 488 and increasing NudC concentrations. Samples were allowed to equilibrate for 15 min at 37 °C and measurements were performed on a Tecan SPARK 10M plate reader in black, flat-bottomed 384-square-well plates. The excitation filter was centered on 485 nm with a bandwidth of 20 nm, and emission filter was centered on 535 nm with a bandwidth of 25 nm. Data were fit to a one-site binding model using OriginPro 2018.

SEC-MALS

To analyze the binding of components and the complex size, we used size exclusion chromatography and multi angle light scattering (SEC-MALS). Proteins at a concentration of 35 μM were mixed in 40 mM Hepes, 150 mM KCl, 5 mM MgCl$_2$ with 1 mM TCEP and 0.05% NaN$_3$ and crosslinked with 0.025% glutardialdehyde at 37 °C for 5 min before the reaction was quenched by addition of excess Tris-HCl pH 8.0. Experiments were conducted with Hsp90α. The samples were subjected to SEC on a Shimdazu HPLC System (Shimadzu, Munich, Germany) with a Superdex 200 Increase 10/300 column and particle size was determined by multi angle light scattering (RF-10AXL fluorescence detector, Shimadzu, Munich, Germany). The Astra 5.3.4 software was used for data analysis (Wyatt Technology, Santa Barbara, USA).

ATPase assay

The Hsp90 ATPase was measured with a regenerative ATPase assay as previously published (Ali et al., 1993; Rutz et al., 2018). Briefly, assay buffer was prepared containing 5.17 mM phosphoenolpyruvate (PEP), 0.43 mM nicotinamidadenine-dinucleotidephosphate (NADH), 5.17 U/mL pyruvate kinase (PK) and 26.06 U/mL lactate dehydrogenase (LDH) in 40 mM Hepes, pH 7.5, 45 mM KCl, 5 mM MgCl$_2$. Assay buffer was mixed 1:1 with proteins diluted in 40 mM Hepes, pH 7.5, 45 mM KCl, 5 mM MgCl$_2$. NudC, Hop, Aha1 and Hsp90α were used at a concentration of 10 μM. The reaction was initiated by the addition of 2.5 mM ATP and the absorption at 340 nm was continuously recorded at 37 °C. After approximately 30 min, radicicol was added at a concentration of 250 μM to fully inhibit Hsp90. The slope after addition of radicicol was subtracted from the slope before Hsp90 inhibition to calculate the Hsp90 ATPase activity. As a control, the co-chaperones were tested in the absence of Hsp90 and the background activity was subtracted from the measurement. Statistical significance was determined by student-t-test (n.s. $p \geq 0.05$; * $p<0.05$, ** $p<0.01$, *** $p<0.001$).

QUANTIFICATION AND STATISTICAL ANALYSIS

Statistical parameters including the exact value of n (replicates) and dispersion and precision measures (mean ± s.d.) are reported in the Figures and Figure Legends. For the quantification of bands in the pull downs, $p < 0.05$ was considered significant. Data analysis was performed in OriginPro 9.1 and in the custom written PAM software. Software used for specific methods.